

FAST EXPANSION INTO HARMONICS ON THE BALL

JOE KILEEL, NICHOLAS F. MARSHALL, OSCAR MICKELIN, AND AMIT SINGER

ABSTRACT. We devise fast and provably accurate algorithms to transform between an $N \times N \times N$ Cartesian voxel representation of a three-dimensional function and its expansion into the ball harmonics, that is, the eigenbasis of the Dirichlet Laplacian on the unit ball in \mathbb{R}^3 . Given $\varepsilon > 0$, our algorithms achieve relative $\ell^1 - \ell^\infty$ accuracy ε in time $\mathcal{O}(N^3(\log N)^2 + N^3|\log \varepsilon|^2)$, while their dense counterparts have time complexity $\mathcal{O}(N^6)$. We illustrate our methods on numerical examples.

1. INTRODUCTION

We consider the problem of expanding discretized functions $f : [-1, 1]^3 \rightarrow \mathbb{C}$ supported on the unit ball $\mathbb{B} = \{x \in \mathbb{R}^3 : \|x\| \leq 1\}$ into the Dirichlet Laplacian eigenfunctions on the unit ball. Given samples of the function f on an $N \times N \times N$ Cartesian grid (we refer to such a discretization as a *volume*), we seek a fast method to obtain the corresponding eigenbasis expansion coefficients. Conversely, given its expansion coefficients we also want a fast method to evaluate the corresponding function f on the grid. The Dirichlet Laplacian eigenfunctions can be written in spherical coordinates (r, θ, ϕ) as

$$\psi_{k,\ell,m}(r, \theta, \phi) = c_{\ell k} j_\ell(\lambda_{\ell k} r) Y_\ell^m(\theta, \phi) \chi_{[0,1]}(r), \quad (1)$$

for $m \in \{-\ell, \dots, \ell\}$, $\ell \in \mathbb{Z}_{\geq 0}$, and $k \in \mathbb{Z}_{>0}$, where the $c_{\ell k}$ are positive normalization constants, j_ℓ are spherical Bessel functions of the first kind, $\lambda_{\ell k}$ is the k -th positive root of j_ℓ , $Y_\ell^m(\theta, \phi)$ are spherical harmonics and $\chi_{[0,1]}$ is an indicator function for $[0, 1)$, which extends the functions to \mathbb{R}^3 ; for precise definitions, see §B in the Supplementary Materials. These eigenfunctions are solutions to the eigenvalue problem

$$-\Delta \psi_{k,\ell,m} = \lambda_{k,\ell,m}^2 \psi_{k,\ell,m} \quad \text{in } \mathbb{B}, \quad (2)$$

$$\psi_{k,\ell,m} = 0 \quad \text{on } \partial\mathbb{B}, \quad (3)$$

where Δ is the Laplacian, see §B.4. These functions are the *ball harmonics* in the sense that they are the standing waves associated with the resonant frequencies of the ball with fixed Dirichlet boundary conditions.

The ball harmonics have a number of beneficial numerical properties, namely they are *orthonormal*, *frequency-ordered*, and *steerable*. Orthonormality stems from the eigenfunction formulation and the fact that the Laplacian is a self-adjoint operator. The frequency-ordering property arises by ordering the eigenfunctions according to their real eigenvalue. It allows one to perform low-pass filtering on volumes expanded into the basis, by retaining the expansion coefficients corresponding to the lowest frequencies and setting the remaining coefficients to zero. Thirdly, the steerability property means that rotations of the basis functions can be efficiently obtained as closed-form linear combinations of the basis functions via Wigner D-matrices [10, Eq. (9.49)]. This allows

2020 *Mathematics Subject Classification*. 65R10, 65D18, 42-04, 33C10, 33C55.

Key words and phrases. Laplacian eigenfunctions, spherical Bessel, spherical harmonics, fast transforms.

Code accompanying this paper is available at https://github.com/oscar Mickelin/fle_3d.

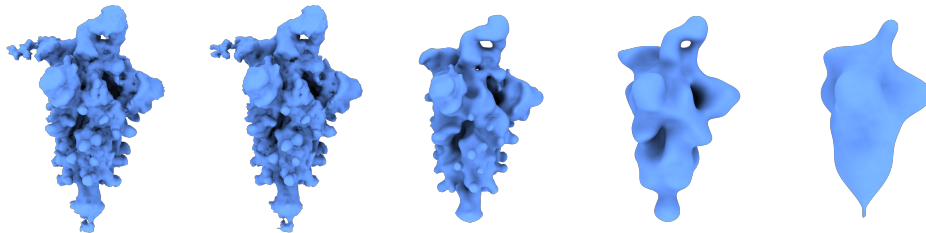


FIGURE 1. Illustration of low-pass filtering in the ball harmonics basis $\psi_{k,\ell,m}$ for volumes of size $128 \times 128 \times 128$. The ground truth volume (leftmost) is a 3D density map of the SARS-CoV-2 Omicron spike glycoprotein complex [24] downloaded from the online electron microscopy data bank [33]. Subsequent panels expand the ground truth volume in ball harmonics and decrease the number of basis functions by dividing the bandlimit by successive factors of 2, so by retaining the basis functions with corresponding $\lambda_{\ell k}$ at most 201.06, 100.53, 50.21, 25.10, respectively, and use 564641, 69545, 8253 and 1007 basis functions, respectively. The volumes are rendered using UCSF ChimeraX [20].

for lossless rotation of volumes expanded into the basis. We illustrate the low-passing property in Figure 1.

1.1. Directly related works. Separable basis functions of the form in (1) with spherical harmonics being the angular components play a crucial role in several imaging techniques, such as cryo-electron microscopy and fluctuation X-ray scattering for 3D reconstruction of molecules [28, 12, 6]. In these inverse problems, experimentally computable quantities provide partial information about the expansion of the solution into such a basis. These hinge on using a basis that is closed under rotations, which by the Peter-Weyl theorem requires angular components represented by spherical harmonics [10, Thm. 8.13]. These basis functions are also a natural choice in other three-dimensional data processing applications, such as geophysics [38], quantum mechanics [3], graph neural networks [18], neuroimaging [17], the solution of partial differential equations [23], cosmology [1, 32, 37, 45], certain types of classification problems [54], acoustical applications generating personalized spatial sound [42], and rotational alignment of three-dimensional objects [31]. In such applications, however, there is freedom in choosing the radial basis functions, and several possible candidates exist. They include Laguerre basis functions [35, 40, 36, 55], Chebyshev polynomials [27], and prolate spheroidal wave functions (also known as Slepian functions) [50].

In many prior works and applications, it is assumed that samples of the 3D function f are available on a spherical grid. Since the basis functions in (1) are separable on a spherical grid, product quadrature can then be used to efficiently compute basis coefficients. Importantly, the setting of the present paper is different, in that we assume access to samples of f only on a Cartesian grid. The separability of the basis functions can therefore not be exploited a priori. That said, the case of radial Laguerre functions (instead of spherical Bessel functions as in this paper) on an unstructured (and not necessarily spherical) grid was previously studied [55]. In our setting of an $N \times N \times N$ Cartesian grid, the computational complexity of the approach of [55] would be $\mathcal{O}(N^{6-3/\epsilon}) \approx \mathcal{O}(N^{4.9})$ (see [55, Thm. 7.1 and the last row of Table 1]), which is significantly higher than that of this article. Overall we are not aware of any provably accurate expansion algorithms on Cartesian grids with time complexity comparable to the algorithms of this paper.

To our best knowledge, the approach taken in this paper is most closely related to the techniques of [49, 2]. However, those papers differ from ours in critical aspects. Specifically they: i) deal with a different problem by solving inverse problems arising from the inhomogeneous Helmholtz equation; ii) assume access to functions on a spherical grid; and iii) are heuristic in nature and do not prove accuracy guarantees of their algorithms. Indeed, besides operating on a Cartesian grid, a major contribution of this article is in proving accuracy guarantees of our basis expansion method. This is done by showing that certain analytical identities for continuous functions f have discrete counterparts when using only samples of f . We show that these discrete counterparts can be interpreted as computing inner products of the samples with all basis functions and, moreover, that they can be evaluated quickly and accurately. The approach in this paper may also have extensions to establishing rigorous fast methods for [35, 40, 36], which use some similar analytical formulas.

All together the present article thus provides a rigorous argument for choosing the radial basis functions in (1), because we contribute fast and accurate basis expansion algorithms for the choice of ball harmonics. As mentioned, the methods have precise accuracy guarantees, and they are linear in the input size (up to logarithmic factors).

In passing, we mention that there are other approaches to function representations on the ball not based on spherical harmonics, which do not enjoy the closure under arbitrary rotations property due to the Peter-Weyl theorem. These include products of Chebyshev polynomials in the radial direction and Fourier modes in the two spherical angular variables in the so-called Double Fourier Sphere method, see [9] for more.

1.2. Connection to 2D work. The three-dimensional functions in (1) are closely related to a certain set of basis functions in two variables: the eigenfunctions of the Dirichlet Laplacian on the unit disk in \mathbb{R}^2 . A subset of the authors previously devised fast algorithms for basis expansion into this two-dimensional basis [39]. The techniques of the present article extend those in [39] to 3D. In doing so, this paper overcomes several significant technical challenges new to the 3D case:

- Firstly, in 2D, the accuracy analysis uses well-known results about the uniform quadrature rule on the circle. In contrast, in 3D, the accuracy analysis involves careful estimates for quadrature grids on the sphere, and a number of special function identities. The error estimates are critical for determining a sufficient number of discretization points to guarantee the 3D algorithms are both fast and accurate.
- Secondly, in 2D, the non-radial computation is handled by the Fast Fourier Transform, which is algebraic, exact and fast in practice. This simplifies both the error analysis and practical implementation. In contrast, in 3D, the algorithms herein use fast approximate spherical harmonics transforms, which introduce additional sources of error as well as implementation tradeoffs between asymptotically fast versus practically fast implementations.
- Thirdly, the increased dimensionality of the problem in 3D compared to 2D poses implementation and computational complexity challenges.

1.3. Supplementary materials. Our work includes expository supplementary material, which precisely describes the notation used in the main paper. While we try to use standard notation throughout, conventions for special functions and operators vary across mathematical communities, which can lead to ambiguity. In particular, the supplementary material sets conventions for spherical coordinates in §B.1, spherical Bessel functions in §B.2, spherical harmonics in §B.3, ball harmonics in §B.4, quadrature rules

on \mathbb{S}^2 in §B.5, spherical harmonic transforms in §B.6, and fast spherical harmonic transforms in §B.7.

2. MAIN RESULT

2.1. Setup. Let $f = (f_{j_1, j_2, j_3})$ be an $N \times N \times N$ volume whose entries represent function values at the points

$$x_{j_1 j_2 j_3} = (hj_1 - 1, hj_2 - 1, hj_3 - 1), \quad \text{where } h = 1/\lfloor (N+1)/2 \rfloor,$$

for $j_1, j_2, j_3 \in \{0, \dots, N-1\}$. More precisely, we assume there is an underlying function (denoted by the same letter, by abuse of notation) $f : [-1, 1]^3 \rightarrow \mathbb{C}$, which is supported on the unit ball \mathbb{B} , such that $f_{j_1 j_2 j_3} = f(x_{j_1 j_2 j_3})$. Let

$$x_1, \dots, x_V \quad \text{and} \quad f_1, \dots, f_V \tag{4}$$

be an enumeration of $(x_{j_1 j_2 j_3})$ and $(f_{j_1 j_2 j_3})$, respectively, where $V = N^3$ is the number of voxels in the volume f . For a given bandlimit $\lambda > 0$, let

$$\psi_1, \dots, \psi_n \tag{5}$$

be an enumeration of the functions $\{\psi_{k, \ell, m} : \lambda_{k, \ell, m} \leq \lambda\}$, where the ball harmonics $\psi_{k, \ell, m}$ and constants $\lambda_{k, \ell, m}$ introduced in (1) are precisely detailed in §B, and the choice of the bandlimit $\lambda > 0$ is discussed in §3.2.

2.2. Ball harmonics transforms. We are interested in devising fast and accurate methods for applying the linear operator $B : \mathbb{C}^n \rightarrow \mathbb{C}^V$ defined by

$$(B\alpha)_j = \sum_{i=1}^n \alpha_i \psi_i(x_j) h^{3/2}, \quad \text{for } j = 1, \dots, V, \tag{6}$$

which maps expansion coefficients to voxelated volumes, and its adjoint $B^* : \mathbb{C}^V \rightarrow \mathbb{C}^n$ defined by

$$(B^*f)_i = \sum_{j=1}^V f_j \overline{\psi_i(x_j)} h^{3/2}, \quad \text{for } i = 1, \dots, n, \tag{7}$$

which maps voxelated volumes to expansion coefficients.

Remark 2.1. In (6) and (7), the normalization constant $h^{3/2}$ is included to make the operator B^*B close to the identity. Observe that

$$(B^*B)_{i,j} = \sum_{k=1}^V \overline{\psi_i(x_k)} \psi_j(x_k) h^3.$$

Since h^3 is the volume of a voxel, the right-hand side is a Riemann sum for the inner product between ψ_i and ψ_j . Therefore, since the functions ψ_i are orthonormal, it approximately equals 1 when $i = j$ and 0 otherwise.

2.3. Main analytic result. Our main analytic result describes the computational complexity of new fast algorithms (see Algorithms 1 and 2 below) for applying the operators B and B^* . The main result is informally stated as follows.

Theorem (Informal Statement). *Assume $n = \mathcal{O}(V)$. Using the algorithms described in this paper, we can apply the operators B and B^* defined in (6) and (7) with relative error ε in $\mathcal{O}(V(\log V)^2 + V|\log \varepsilon|^2)$ operations.*

See Theorem 3.1 for a precise statement of this result. The fast algorithms for applying B^* and B are detailed in Algorithms 1 and 2, respectively.

3. ALGORITHMS

This section presents the paper's fast algorithms for applying approximations to the operators B^* and B in Algorithms 1–2, respectively. We start by giving a precise statement of our main analytic result, which provides error guarantees and the computational complexity for the algorithms.

Theorem 3.1. *Assume $\lambda \leq 6^{1/3}\pi^{2/3}[(V^{1/3} + 1)/2]$ and $\varepsilon > 0$ is a user-specified parameter satisfying $|\log_2 \varepsilon| \leq 5.3V^{1/3}$. Then Algorithms 1–2 take $\mathcal{O}(V(\log V)^2 + V|\log \varepsilon|^2)$ operations and their outputs \tilde{B}^*f and $\tilde{B}\alpha$ satisfy the accuracy bounds*

$$\|\tilde{B}^*f - B^*f\|_{\ell^\infty} \leq \varepsilon\|f\|_{\ell^1} \quad \text{and} \quad \|\tilde{B}\alpha - B\alpha\|_{\ell^\infty} \leq \varepsilon\|\alpha\|_{\ell^1}, \quad (8)$$

for all inputs f and α .

The proof of Theorem 3.1 is in Appendix A. Several immediate remarks are helpful.

Remark 3.1 (Other grids). We remark that the proof of Theorem 3.1 carries through for points x_j and samples f_j on arbitrary grids, provided $x_j \leq 1$. Algorithmically, this is achieved by using a type 3 (nonuniform to nonuniform) NUFFT transform (see [5]) in Step 1 and 3 of Algorithms 1 and 2, respectively.

Remark 3.2 (Choice of norms). Bounds of the type in (8) using ℓ^1 - ℓ^∞ bounds are common in the analysis of algorithms that use the non-uniform fast Fourier transform (NUFFT), see for example [4, Eq. (9)]. Since the algorithms of this paper use NUFFT, we obtain the ℓ^1 - ℓ^∞ form of (8). However, we note that Theorem 3.1 also ensures accuracy with ℓ^2 - ℓ^2 bounds with the same asymptotic computational complexity. Since

$$\frac{\|\tilde{B}^*f - B^*f\|_{\ell^2}}{\|f\|_{\ell^2}} \leq \sqrt{nV} \frac{\|\tilde{B}^*f - B^*f\|_{\ell^\infty}}{\|f\|_{\ell^1}},$$

running Algorithms 1–2 with accuracy parameter ε/\sqrt{nV} ensures accuracy $\|\tilde{B}^*f - B^*f\|_{\ell^2} \leq \varepsilon\|f\|_{\ell^2}$ in time $\mathcal{O}(V(\log V)^2 + V|\log \varepsilon/\sqrt{nV}|^2) = \mathcal{O}(V(\log V)^2 + V|\log \varepsilon|^2)$, using the fact that $n = \mathcal{O}(V)$ with the choice of bandlimit in Theorem 3.1 (see §3.2).

Remark 3.3 (Dense matrix operators). When the number of basis functions n is on the order of the number of voxels V , a direct application of B or B^* requires forming a matrix with order V^2 elements and then matrix-vector products involve order V^2 operations. For example, if a $100 \times 100 \times 100$ volume is given, then $V = 10^6$. Storing a dense matrix with $V^2 = 10^{12}$ entries using single precision floating point numbers would require 4 terabytes of storage. If this matrix cannot fit in memory, it either needs to be constructed online or moved in and out of memory, creating additional implementation challenges.

Remark 3.4 (No smoothness assumptions). Theorem 3.1 does not make any smoothness assumptions on the input function f . The fact that the algorithm works for noisy inputs is essential for applications such as low-pass filtering or cryo-electron tomography, where measurement data is heavily corrupted by noise, so we cannot even assume the continuity of the underlying function f . Even in the absence of noise, data is not necessarily smooth, due e.g. to sharp boundaries, corners, or cusps. We note however that if the input f_{j_1, j_2, j_3} were to consist of samples from a sufficiently smooth function, then a fast algorithm could be created by interpolating the volume data f_{j_1, j_2, j_3} from the given Cartesian grid onto a product grid of the form $\{r_1, \dots, r_R\} \times \{\theta_1, \dots, \theta_T\} \times \{\phi_1, \dots, \phi_P\}$ in the radial and spherical variables. Because of the separable structure of the basis functions in (1), a product-structured quadrature rule could then be applied to compute the basis coefficients with reduced complexity. Further the product quadrature could be

computed using fast spherical harmonic transforms in the spherical variables. Assuming R, T, P are $\mathcal{O}(N)$, then the resulting computational complexity would be the same as our method, that is $\mathcal{O}(N^3(\log N)^2)$. That said, the behavior of this algorithm, especially for noisy volumes, would be unpredictable. The final accuracy of the basis coefficients would be related to the accuracy of the interpolation step and, therefore, to the smoothness of the underlying function f that provides the discretizations f_{j_1, j_2, j_3} and noise. Hence this straightforward algorithm is of limited utility to various applications of interest. In contrast, the methods described in this paper are simply fast ways to apply the matrix operators B and B^* defined in (6) and (7), respectively, and their ℓ^1 - ℓ^∞ accuracy guarantees hold for all inputs.

Remark 3.5. (Real-valued basis transform) Statements analogous to Theorem 3.1 hold for the real-valued basis functions of (79). Our code provides the option of choosing between the real- and complex-valued bases, as well as converting computed basis coefficients between real and complex form via the transformation in (79).

3.1. Key analytic identities. The key idea behind the algorithms is the analytic identities described in this section. With the notation from (63), we write the basis functions $\psi_{k, \ell, m}$ in (75) as

$$\psi_{k, \ell, m}(x) = c_{\ell k} j_\ell(\lambda_{\ell k} r_x) Y_\ell^m(\gamma_x) \chi_{[0,1]}(r_x). \quad (9)$$

We will likewise write the frequency variable ω for the Fourier-transform of $\psi_{k, \ell, m}$ in spherical coordinates $\omega = r_\omega \gamma_\omega$, where $r_\omega \geq 0$ and $\gamma_\omega \in \mathbb{S}^2$, see §B.1.

We are studying expansions into the ball harmonics, i.e., into the basis defined by (9), for $m \in \{-\ell, \dots, \ell\}$, $\ell \in \mathbb{Z}_{\geq 0}$, and $k \in \mathbb{Z}_{>0}$. Our fast algorithms build on the following identity

$$e^{i\omega \cdot x} = 4\pi \sum_{\ell'=0}^{\infty} \sum_{m'=-\ell'}^{\ell'} i^{\ell'} j_{\ell'}(r_x r_\omega) Y_{\ell'}^{m'}(\gamma_x) \overline{Y_{\ell'}^{m'}(\gamma_\omega)}, \quad (10)$$

which is known as the plane-wave expansion [10, §4.7.4]. The following result is a straightforward consequence of the plane-wave expansion.

Lemma 3.1. *Writing $\omega = r_\omega \gamma_\omega$ as in (63), the Fourier transform of ψ satisfies*

$$\widehat{\psi}_{k, \ell, m}(\omega) = \left(4\pi (-i)^\ell \int_0^1 c_{\ell k} j_\ell(\lambda_{\ell k} r_x) j_\ell(r_x r_\omega) r_x^2 dr_x \right) Y_\ell^m(\gamma_\omega). \quad (11)$$

Proof. Using (10) in the definition of the Fourier transform results in

$$\begin{aligned} \widehat{\psi}_{k, \ell, m}(\omega) &= \int_{\mathbb{R}^3} \psi_{k, \ell, m}(x) e^{-i\omega \cdot x} dx \\ &= 4\pi \int_{\mathbb{R}^3} \psi_{k, \ell, m}(x) \left(\sum_{\ell'=0}^{\infty} \sum_{m'=-\ell'}^{\ell'} (-i)^{\ell'} j_{\ell'}(r_x r_\omega) \overline{Y_{\ell'}^{m'}(\gamma_x)} Y_{\ell'}^{m'}(\gamma_\omega) \right) dx \\ &= 4\pi \int_{\mathbb{R}^3} c_{\ell k} j_\ell(\lambda_{\ell k} r_x) Y_\ell^m(\gamma_x) \chi_{[0,1]}(r_x) \\ &\quad \times \sum_{\ell'=0}^{\infty} \sum_{m'=-\ell'}^{\ell'} (-i)^{\ell'} j_{\ell'}(r_x r_\omega) \overline{Y_{\ell'}^{m'}(\gamma_x)} Y_{\ell'}^{m'}(\gamma_\omega) dx \\ &= \left(4\pi (-i)^\ell \int_0^1 c_{\ell k} j_\ell(\lambda_{\ell k} r_x) j_\ell(r_x r_\omega) r_x^2 dr_x \right) Y_\ell^m(\gamma_\omega), \end{aligned}$$

where the last step used the orthogonality of the spherical harmonics from (69). We note that interchanging the integral over the sphere with the summations in the calculations

is justified since $j_\ell(z)$ decays super exponentially when z is fixed and $\ell \rightarrow \infty$ (see (66) and [11, Eq. (10.19.1)]), so Fubini's Theorem applies. \square

The lemma implies the next theorem, which is the basis of our fast algorithms.

Theorem 3.2. *Let $f = \sum_{(k,\ell,m) \in \mathcal{I}} \alpha_{k,\ell,m} \psi_{k,\ell,m}$ for a finite index set*

$$\mathcal{I} \subseteq \{(k, \ell, m) : m \in \{-\ell, \dots, \ell\}, \ell \in \mathbb{Z}_{\geq 0}, k \in \mathbb{Z}_{>0}\},$$

and define

$$\beta_{\ell,m}(\rho) = \frac{\rho^\ell}{4\pi} \int_{\mathbb{S}^2} \widehat{f}(\rho\gamma_\omega) \overline{Y_\ell^m(\gamma_\omega)} d\sigma(\gamma_\omega). \quad (12)$$

It then holds that

$$\alpha_{k,\ell,m} = c_{\ell k} \beta_{\ell,m}(\lambda_{\ell k}), \quad \text{for all } (k, \ell, m) \in \mathcal{I}. \quad (13)$$

Proof. Using (11), we obtain

$$\begin{aligned} \beta_{\ell,m}(\rho) &= \frac{\rho^\ell}{4\pi} \int_{\mathbb{S}^2} \sum_{(k',\ell',m') \in \mathcal{I}} \alpha_{k',\ell',m'} \widehat{\psi}_{k',\ell',m'}(\rho\gamma_\omega) \overline{Y_\ell^m(\gamma_\omega)} d\sigma(\gamma_\omega) \\ &= \sum_{(k',\ell',m') \in \mathcal{I}} \alpha_{k',\ell',m'} \delta_{\ell\ell'} \delta_{mm'} \int_0^1 c_{\ell k'} j_\ell(\lambda_{\ell k'} r_x) j_\ell(r_x \rho) r_x^2 dr_x. \end{aligned} \quad (14)$$

By orthogonality of the spherical Bessel functions, it follows that

$$\begin{aligned} \beta_{\ell,m}(\lambda_{\ell k}) &= \sum_{(k',\ell',m') \in \mathcal{I}} \alpha_{k',\ell',m'} \delta_{\ell\ell'} \delta_{mm'} \int_0^1 c_{\ell k'} j_\ell(\lambda_{\ell k'} r_x) j_\ell(\lambda_{\ell k} r_x) r_x^2 dr_x \\ &= \sum_{(k',\ell',m') \in \mathcal{I}} \frac{\alpha_{k',\ell',m'}}{c_{\ell k}} \delta_{kk'} \delta_{\ell,\ell'} \delta_{mm'} = \frac{\alpha_{k,\ell,m}}{c_{\ell k}}, \end{aligned} \quad (15)$$

for any (k, ℓ, m) in \mathcal{I} . \square

3.2. Choice of bandlimit. An important parameter in the algorithm is the choice of bandlimit for the expansion. In this section, we derive a maximum bandlimit based on equating the number of pixels and basis functions.

Let $V = V(h)$ be the number of voxels of size $h \times h \times h$ contained in the unit ball, where $h = 1/\lfloor(N+1)/2\rfloor$ for positive integer N . By [26] we have

$$V(h) = \frac{4\pi}{3} h^{-3} + \mathcal{O}\left(h^{-\frac{21}{16}-\varepsilon}\right), \quad \text{as } h \rightarrow 0, \quad (16)$$

for any fixed $\varepsilon > 0$. The number of Dirichlet eigenvalues of the Laplacian on the unit-ball in \mathbb{R}^3 that are less than or equal to λ^2 is by Weyl's law [25]:

$$\mathcal{N}(\lambda) = \frac{2}{9\pi} \lambda^3 - \frac{1}{4} \lambda^2 + o(\lambda^2) \quad \text{as } \lambda \rightarrow \infty. \quad (17)$$

Equating $V(h) = \mathcal{N}(\lambda)$ gives a suitable bandlimit condition since beyond this bandlimit, there will be more basis functions than voxels. For simplicity, we equate the leading-order terms of $V(h)$ and $\mathcal{N}(\lambda)$, which gives

$$\lambda = 6^{1/3} \pi^{2/3} \frac{1}{h}. \quad (18)$$

Since we discarded the second term in (17), this estimate on λ is a slight underestimate compared to equating the exact expressions of $V(h)$ and $\mathcal{N}(\lambda)$. We remark that, in practice, it may be advantageous to compute expansions using a fraction of the bandlimit (18), say, half the maximum bandlimit if noise in the data may make the high-frequency

coefficients less informative; in any case, choosing λ on the order of h^{-1} such that it is less than (18) is reasonable.

3.3. Precise setting. We now make the setting of Theorem 3.1 precise. We must specify the enumerations (4) and (5) in the definitions of the operators B and B^* . We fix the enumeration of the $V = N^3$ voxels to be lexicographic, with no loss of generality. For the ball harmonics we switch between indexing them by the triples (k, ℓ, m) and enumerating them by sequential indices

$$\psi_1, \psi_2, \dots, \psi_n, \quad (19)$$

after fixing an ordering of the (k, ℓ, m) triples. The triples are ordered by sorting the ball harmonics via increasing values of $\lambda_{\ell k}$ with ties broken in the order $m = 0, -1, 1, -2, 2, \dots, -\ell, \ell$. Optionally, our implementation lets users specify integers L and K , and consider only basis triples with $\ell \leq L$ and $k \leq K$. The values of the indices (k, ℓ, m) corresponding to the sequential ordering are denoted by

$$k_i, \ell_i, m_i, \quad \text{for } i = 1, \dots, n. \quad (20)$$

For convenience, for a given bandlimit λ (see Section 3.2 for one choice of λ) we let

$$\lambda_1 \leq \dots \leq \lambda_n, \quad (21)$$

be an enumeration of the $\lambda_{\ell k}$ with magnitude at most λ , where the $\lambda_{\ell k}$ are repeated according to their multiplicity.

We will refer to the maximum values of ℓ and k that correspond to a $\lambda_{\ell k} \leq \lambda$ by

$$L = \max\{\ell \in \mathbb{Z}_{\geq 0} : \text{there exists } k \in \mathbb{Z}_{> 0} \text{ with } \lambda_{\ell k} \leq \lambda\}, \quad (22)$$

$$K = \max\{k \in \mathbb{Z}_{> 0} : \text{there exists } \ell \in \mathbb{Z}_{\geq 0} \text{ with } \lambda_{\ell k} \leq \lambda\}. \quad (23)$$

By [16, Eq. 1.6], the roots $\lambda_{\ell k}$ satisfy $\lambda_{\ell k} > \ell + 1/2 + k\pi - \pi/2 + 1/2$. Therefore $\lambda_{\ell k} > \ell$ and $\lambda_{\ell k} > k$, which imply the (slightly pessimistic) bounds

$$L \leq \lambda \quad \text{and} \quad K \leq \lambda. \quad (24)$$

3.4. Fast algorithms. This section leverages the analytical identities of Section 3.1 to produce the fast algorithms of Theorem 3.1.

The overall idea of the algorithms is to compute the basis expansion coefficients by using (12) and (13). However, these identities only apply to continuous functions $f : [-1, 1]^3 \rightarrow \mathbb{C}$, whereas Theorem 3.1 assumes a discretized input. A main insight of our algorithms is that (12) and (13) have discrete counterparts, where replacing the continuous Fourier-transforms by the discrete Fourier-transforms approximately replaces the continuous basis coefficients $\alpha_{k, \ell, m}$ in (13) by the vector $B^* f$ from (7). It may not be immediately clear that a discrete version of these identities would lead to numerically accurate code. However, a careful analysis proves that the resulting algorithms are both fast and accurate when using enough discretization points.

Crucially, we obtain the computational complexity of Theorem 3.1 by not computing (12) and (13) for *all* $\lambda_{\ell k}$, but rather only for a smaller set of points ρ_q . We then extend the result to all $\lambda_{\ell k}$ via 1D polynomial interpolation. In particular, with λ_1 and λ_n as defined in (21), we take the smaller set of points to be Chebyshev nodes of the first kind on the interval $[\lambda_1, \lambda_n]$, i.e.,

$$\rho_q = \frac{\lambda_n - \lambda_1}{2} \cos\left(\frac{2q+1}{Q} \cdot \frac{\pi}{2}\right) + \frac{\lambda_1 + \lambda_n}{2}, \quad q = 0, \dots, Q-1. \quad (25)$$

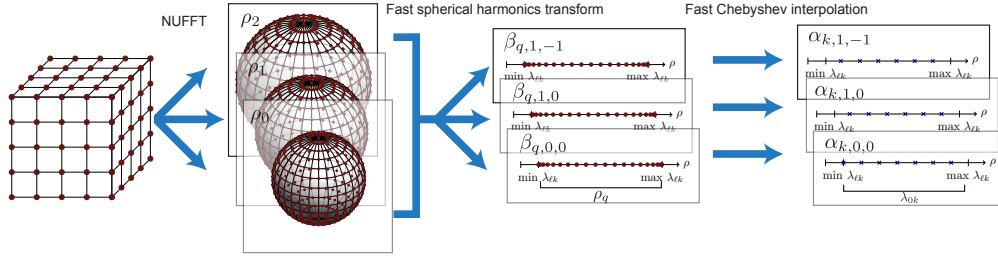


FIGURE 2. Illustration of the algorithm for applying B^* , where the arrows correspond to the steps of the algorithm.

The one-dimensional polynomial interpolating the function values y_q from the source points ρ_q to the target point x is then

$$P(x) = \sum_{q=0}^{Q-1} y_q u_q(x) \text{ where } u_q(x) = \frac{\prod_{r \neq q} (x - \rho_r)}{\prod_{r \neq q} (\rho_q - \rho_r)}, \text{ for } q = 0, \dots, Q-1. \quad (26)$$

All together, the fast procedure for applying \tilde{B}^* is as follows (see also Figure 2):

- (1) Use the nonuniform fast Fourier transform (NUFFT) to approximately evaluate \hat{f} in (12) on a grid with Chebyshev nodes in the radial direction and suitable spherical nodes.
- (2) Use a fast spherical harmonics transform to approximate the integral in (12) at Chebyshev nodes ρ .
- (3) Use fast interpolation from the Chebyshev nodes ρ to the points λ_{l_k} to approximate (13).

Note that each of the three steps above involved in applying the approximation to B^* are linear transforms whose adjoints can be applied with the same low computational complexity. For example, the adjoint of a type-I NUFFT is a type-II NUFFT. Thus, approximately applying the operator B can be achieved by applying each of the adjoints in the reverse order, with the same overall computational complexity as the approximate application of B^* . We summarize the two algorithms in Algorithms 1 and 2.

4. KEY DISCRETE RESULTS

The most important part of both the proof of Theorem 3.1 and the practical implementation of Algorithms 1 and 2 is ensuring that the scaling of the number of discretization nodes is correct. In this section, we derive a bound on the number of nodes that achieves a desired level of precision with the complexity written in Theorem 3.1.

4.1. Number of radial nodes. Our first lemma states the number of radial nodes required to obtain a prescribed accuracy with the desired complexity.

Lemma 4.1. *Let the number of radial Chebyshev nodes in (25) be*

$$Q = \left\lceil \max\{5.3V^{1/3}, \log_2 \eta^{-1}\} \right\rceil. \quad (27)$$

Write $x_j = r_{x_j} \gamma_{x_j}$ as in (63), with $0 \leq r_{x_j} \leq 1$. Let $P_{\ell, m, j}$ be the degree $Q-1$ interpolating polynomial in (26) satisfying

$$P_{\ell, m, j}(\rho_q) = j_\ell(r_{x_j} \rho_q) \overline{Y_\ell^m(\gamma_{x_j})},$$

Algorithm 1: Fast application of \tilde{B}^* ,

Input: Discretized volume $f \in \mathbb{C}^V$, bandlimit λ , and precision ε .

Constants: Maximum number n of basis functions, ε^{dis} given by (54) below, ε^{nuf} , ε^{fsh} and ε^{in} given by (50) below, $S = \lceil \max\{2e6^{1/3}\pi^{2/3}[(V^{1/3} + 1)/2], 4|\log_2(27.6\varepsilon^{\text{dis}})|\} \rceil$, and $Q = \lceil \max\{5.3V^{1/3}, |\log_2 \varepsilon^{\text{dis}}|\} \rceil$.

Output: $\tilde{B}^*f = \alpha \in \mathbb{C}^n$ approximating B^*f to relative error ε (see Theorem 3.1).

- 1 Let ρ_q and $\gamma_{s,t}$ be given by (25) and (81), respectively. Using the NUFFT, calculate

$$a_{qst} = \sum_{j=1}^V f_j e^{-ix_j \cdot \rho_q \gamma_{s,t}},$$

with relative error ε^{nuf} , where $q \in \{0, \dots, Q-1\}$, $s \in \{0, \dots, S\}$ and $t \in \{0, \dots, S-1\}$.

- 2 Using a fast spherical harmonics transform, calculate

$$\beta_{q,\ell,m} = \frac{i^\ell}{4\pi} \sum_{s=0}^S \sum_{t=0}^{S-1} w_s a_{qst} \overline{Y_\ell^m(\gamma_{s,t})},$$

for $q \in \{0, \dots, Q-1\}$, $\ell \in \{0, \dots, L\}$ and $m \in \{-\ell, \dots, \ell\}$, where the w_s are quadrature weights given by (82).

- 3 For $\ell = 0, \dots, L$, and $m = -\ell, \dots, \ell$, use fast Chebyshev interpolation to calculate

$$\alpha_i = \sum_{q=0}^{Q-1} c_i \beta_{q\ell_i m_i} u_q(\lambda_i) h^{3/2},$$

where $u_q(\cdot)$ are the interpolating polynomials given by (26).

for $q \in \{0, \dots, Q-1\}$, where ρ_q are the Chebyshev nodes for $[\lambda_1, \lambda_n]$ defined in (25) and λ_n satisfies (18). Then,

$$|P_{\ell,m,j}(\rho_k) - j_\ell(r_{x_j} \rho_k) \overline{Y_\ell^m(\gamma_{x_j})}| \leq \eta,$$

for all $\rho \in [\lambda_1, \lambda_n]$, $\ell \in \{0, \dots, L\}$, $m \in \{-\ell, \dots, \ell\}$, and $j \in \{1, \dots, V\}$, where L is defined in (22).

Proof of Lemma 4.1. Let $h : [a, b] \rightarrow \mathbb{R}$ be a smooth function, and P be the polynomial that interpolates h at Q Chebyshev nodes. Then, the residual $R(\rho) = h(\rho) - P(\rho)$ satisfies

$$|R(\rho)| \leq \frac{C_Q}{Q!} \left(\frac{b-a}{4} \right)^Q, \quad \text{where } C_Q := \max_{\rho \in [a,b]} |h^{(Q)}(\rho)|$$

for all $\rho \in [a, b]$; see [47, Lemma 2.1]. Set

$$[a, b] := [\lambda_1, \lambda_m], \quad \text{and} \quad h(\rho) := j_\ell(r_{x_j} \rho) \overline{Y_\ell^m(\gamma_{x_j})}.$$

First, we estimate $|R(\rho)|$ by

$$|R(\rho)| \leq \frac{C_Q}{Q!} \left(\frac{\lambda_m - \lambda_1}{4} \right)^Q \leq \frac{C_Q}{Q!} \left(\left(\frac{\sqrt{3}\pi}{16} \right)^{2/3} (V^{1/3} + 1) \right)^Q,$$

Algorithm 2: Fast application of \tilde{B} .**Input:** Coefficients $\alpha \in \mathbb{C}^n$, bandlimit λ , and precision ε .**Constants:** Number of voxels V , ε^{dis} given by (61), $\varepsilon^{\text{in}}, \varepsilon^{\text{fsh}}$ and ε^{nuf} given by (57), $S = \lceil \max\{2e6^{1/3}\pi^{2/3}\lfloor (V^{1/3} + 1)/2 \rfloor, 4\lceil \log_2(27.6\varepsilon^{\text{dis}}) \rceil\} \rceil$, and $Q = \lceil \max\{5.3V^{1/3}, \lceil \log_2 \varepsilon^{\text{dis}} \rceil\} \rceil$.**Output:** $f \in \mathbb{C}^V$ approximating $B\alpha$ to relative error ε (see Theorem 3.1)

- 1 For $q = 0, \dots, Q - 1$, $\ell = 0, \dots, L$, and $m = -\ell, \dots, \ell$, use the adjoint of fast Chebyshev interpolation to apply

$$\beta_{q,\ell,m}^* = \sum_{\substack{i:\ell_i=\ell, \\ m_i=m}} c_i \alpha_i u_q(\lambda_i) h^{3/2},$$

where the sum is over i such that the corresponding sequential indices from (20) satisfy $\ell_i = \ell$ and $m_i = m$.

- 2 Using a fast spherical harmonics transform, calculate

$$a_{qst}^* = \sum_{\ell=0}^L \frac{(-\ell)^\ell}{4\pi} \sum_{m=-\ell}^{\ell} w_s \beta_{q,\ell,m}^* Y_\ell^m(\gamma_{s,t}),$$

where $q \in \{0, \dots, Q - 1\}$, $s \in \{0, \dots, S\}$, $t \in \{0, \dots, S - 1\}$ and the w_s are quadrature weights given by (82).

- 3 With ρ_q given in (25) and $\gamma_{s,t}$ in (81), use the NUFFT to calculate the quantities

$$f_j = \sum_{q=0}^{Q-1} \sum_{s=0}^S \sum_{t=0}^{S-1} a_{qst}^* e^{tx_j \cdot \rho_q \gamma_{s,t}},$$

for each $j = 1, \dots, V$.

where we used the fact that

$$\lambda_n - \lambda_1 \leq \lambda_n \leq \left(\frac{\sqrt{3}\pi}{2} \right)^{2/3} (V^{1/3} + 1);$$

see §3.2 for the last inequality. Next, we estimate

$$C_Q := \max_{\rho \in [\lambda_1, \lambda_n]} \left| \frac{\partial^Q}{\partial \rho^Q} (j_\ell(r_{x_j} \rho)) \overline{Y_\ell^m(\gamma_{x_j})} \right|,$$

by expanding the function $j_\ell(r_{x_j} \rho)$ using the integral identity in [11, Eq. 10.54.2] and obtain

$$\begin{aligned} \left| \frac{\partial^Q}{\partial \rho^Q} j_\ell(r_{x_j} \rho) \right| &= \left| \frac{1}{2} \int_0^\pi \frac{\partial^Q}{\partial \rho^Q} \left(e^{ir_{x_j} \rho \cos(\theta)} P_\ell(\cos \theta) \sin \theta \right) d\theta \right| \\ &= \left| \frac{1}{2} \int_0^\pi (ir_{x_j} \cos(\theta))^Q e^{ir_{x_j} \rho \cos(\theta)} P_\ell(\cos \theta) \sin \theta d\theta \right| \\ &\leq \frac{1}{2} \int_0^\pi |P_\ell(\cos \theta)| \sin \theta d\theta = \frac{1}{2} \int_{-1}^1 |P_\ell(x)| dx \\ &\leq \frac{1}{2} \sqrt{\frac{2}{2\ell + 1}} \sqrt{2} = \frac{1}{\sqrt{2\ell + 1}}, \end{aligned}$$

where the first inequality follows from the triangle inequality and the fact that $0 \leq r_{x_j} \leq 1$. The second inequality follows from Cauchy-Schwarz and the fact that $\sqrt{2}/(2\ell + 1)$ is

the L^2 -norm of P_ℓ on the interval $[-1, 1]$, see [11, Table 18.3.1]. Combining this with the bound $|Y_\ell^m(\gamma_{x_j})| \leq \sqrt{\frac{2\ell+1}{4\pi}}$ from (70), we obtain

$$C_Q \leq \frac{1}{\sqrt{4\pi}}.$$

In combination with Stirling's approximation [46], it follows that

$$\begin{aligned} |R(\rho)| &\leq \frac{1}{\sqrt{4\pi}Q!} \left(\left(\frac{\sqrt{3}\pi}{16} \right)^{\frac{2}{3}} (V^{\frac{1}{3}} + 1) \right)^Q \\ &\leq \frac{1}{\sqrt{8Q\pi}} \left(\frac{e}{Q} \left(\frac{\sqrt{3}\pi}{16} \right)^{\frac{2}{3}} (V^{\frac{1}{3}} + 1) \right)^Q. \end{aligned} \quad (28)$$

We note that $V^{1/3} \geq 1$, $2e \left(\frac{\sqrt{3}\pi}{16} \right)^{2/3} \leq 2.65$ and $\frac{1}{\sqrt{8Q\pi}} \leq 1$. Therefore, in order to achieve error $|R(\rho)| \leq \eta$, it suffices to set Q such that

$$\eta \geq \left(\frac{2.65V^{1/3}}{Q} \right)^Q. \quad (29)$$

Setting $\frac{2.65V^{1/3}}{Q} = 1/2$ and solving for Q gives $Q = 5.3V^{1/3}$. This implies that choosing $Q \geq \max\{5.3V^{1/3}, \log_2 \eta^{-1}\}$ is sufficient to achieve error less than η . \square

Remark 4.1. (Optimizing the bound for Q) The bounds used in the proof of Lemma 4.1 to show the asymptotic behavior of Q are slightly conservative. In practice, we can numerically obtain smaller values of Q through (28), by choosing the smallest integer Q satisfying

$$\frac{1}{\sqrt{4\pi}Q!} \left(\left(\frac{\sqrt{3}\pi}{16} \right)^{2/3} (V^{1/3} + 1) \right)^Q \leq \eta.$$

4.2. Number of spherical nodes. Our second lemma similarly gives the number of spherical nodes needed to obtain a prescribed accuracy with the desired complexity.

Lemma 4.2. *Let $\eta > 0$ be given. With $\gamma_{s,t}, w_s$ from (81) and (82), L from (22) and λ_1, λ_n from (21), let $\rho \in [\lambda_1, \lambda_n]$ and define*

$$R_{\ell,m,j}(\rho) = \left| \frac{i^\ell}{4\pi} \sum_{s=0}^S \sum_{t=0}^{S-1} w_s \overline{Y_\ell^m(\gamma_{s,t})} e^{-ix_j \cdot \rho \gamma_{s,t}} - j_\ell(r_{x_j} \rho) \overline{Y_\ell^m(\gamma_{x_j})} \right|,$$

where $x_j = r_{x_j} \gamma_{x_j}$ is written in the form in (63) with $0 \leq r_{x_j} \leq 1$. If λ_n satisfies (18) and S satisfies

$$S \geq \lceil \max\{2e6^{1/3}\pi^{2/3}[(V^{1/3} + 1)/2], 4\log_2(27.6\eta^{-1})\} \rceil, \quad (30)$$

then $R_{\ell,m,j}(\rho) \leq \eta$, for $\ell \in \{0, \dots, L\}$, $m \in \{-\ell, \dots, \ell\}$, and $j \in \{1, \dots, V\}$.

Proof of Lemma 4.2. Assume S satisfies (30). Let

$$g_{\ell,m,j}(\rho, \gamma) = \frac{i^\ell}{4\pi} \overline{Y_\ell^m(\gamma)} e^{-ix_j \cdot \rho \gamma}. \quad (31)$$

We want to show that

$$R_{\ell,m,j}(\rho) = \left| \sum_{s=0}^S \sum_{t=0}^{S-1} w_s g_{\ell,m,j}(\rho, \gamma_{s,t}) - j_\ell(r_{x_j} \rho) \overline{Y_\ell^m(\gamma_{x_j})} \right| < \eta. \quad (32)$$

Notice that the sum in (32) is a discretization of the integral

$$\int_{\mathbb{S}^2} g_{\ell,m,j}(\rho, \gamma) d\sigma(\gamma) = j_{\ell}(r_{x_j}\rho) \overline{Y_{\ell}^m(\gamma_{x_j})}, \quad (33)$$

where this exact expression for the integral follows from (10). For fixed j and ρ , we define the constants

$$\alpha_{m',\ell'} = 4\pi(-i)^{\ell'} j_{\ell'}(r_{x_j}\rho) \overline{Y_{\ell'}^{m'}(\gamma_{x_j})}, \quad (34)$$

and use the plane-wave expansion in (10) to write

$$e^{-i\rho\gamma \cdot x_j} = \sum_{\ell'=0}^{\infty} \sum_{m'=-\ell'}^{\ell'} \alpha_{m',\ell'} Y_{\ell'}^{m'}(\gamma). \quad (35)$$

By (30) and (24), we have $L \leq S/2$. Recall from (84) that the quadrature rule defined by (81) and (82) is exact for integrals corresponding to inner products of bandlimited functions on the sphere when $L \leq S/2$. This gives

$$\begin{aligned} R_{\ell,m,j}(\rho) &= \left| \sum_{s=0}^S \sum_{t=0}^{S-1} w_s \frac{i^{\ell}}{4\pi} e^{-ix_j \cdot \rho \gamma_s} \overline{Y_{\ell}^m(\gamma_{s,t})} - \int_{\mathbb{S}^2} \frac{i^{\ell}}{4\pi} e^{-ix_j \cdot \rho \gamma_{\omega}} \overline{Y_{\ell}^m(\gamma_{\omega})} d\sigma(\gamma_{\omega}) \right| \\ &= \left| \sum_{s=0}^S \sum_{t=0}^{S-1} w_s \frac{i^{\ell}}{4\pi} \sum_{\ell'=0}^{\infty} \sum_{m'=-\ell'}^{\ell'} \alpha_{m',\ell'} Y_{\ell'}^{m'}(\gamma_{s,t}) \overline{Y_{\ell}^m(\gamma_{s,t})} \right. \\ &\quad \left. - \int_{\mathbb{S}^2} \frac{i^{\ell}}{4\pi} \sum_{\ell'=0}^{\infty} \sum_{m'=-\ell'}^{\ell'} \alpha_{m',\ell'} Y_{\ell'}^{m'}(\gamma_{\omega}) \overline{Y_{\ell}^m(\gamma_{\omega})} d\sigma(\gamma_{\omega}) \right| \quad (36) \\ &= \left| \sum_{s=0}^S \sum_{t=0}^{S-1} \left(\sum_{\ell'=\lfloor S/2 \rfloor + 1}^{\infty} \sum_{m'=-\ell'}^{\ell'} \frac{i^{\ell}}{4\pi} w_s \alpha_{m',\ell'} Y_{\ell'}^{m'}(\gamma_{s,t}) \overline{Y_{\ell}^m(\gamma_{s,t})} \right) \right. \\ &\quad \left. - \sum_{\ell'=\lfloor S/2 \rfloor + 1}^{\infty} \sum_{m'=-\ell'}^{\ell'} \frac{i^{\ell}}{4\pi} \alpha_{m',\ell'} \int_{\mathbb{S}^2} Y_{\ell'}^{m'}(\gamma_{\omega}) \overline{Y_{\ell}^m(\gamma_{\omega})} d\sigma(\gamma_{\omega}) \right|. \end{aligned}$$

We proceed by bounding the coefficients $\alpha_{m',\ell'}$ in order to show that the preceding sum is bounded in magnitude by η . By the definition of $\alpha_{m',\ell'}$ in (34)

$$\begin{aligned} \left| \frac{i^{\ell}}{4\pi} \alpha_{m',\ell'} \right| &= \left| j_{\ell'}(r_{x_j}\rho) \overline{Y_{\ell'}^{m'}(\gamma_{x_j})} \right| \leq \frac{\sqrt{\pi}}{2} \frac{\left(\frac{r_{x_j}\rho}{2}\right)^{\ell'}}{\Gamma(\ell'+3/2)} \sqrt{\frac{2\ell'+1}{4\pi}} \\ &\leq \frac{\sqrt{\pi}}{2} \sqrt{\frac{\ell'+3/2}{2\pi}} \left(\frac{e}{\ell'+3/2}\right)^{\ell'+3/2} \left(\frac{r_{x_j}\rho}{2}\right)^{\ell'} \sqrt{\frac{2\ell'+1}{4\pi}} \quad (37) \\ &= \frac{e^{3/2}}{4\sqrt{2\pi}} \frac{\sqrt{2\ell'+1}}{\ell'+3/2} \left(\frac{er_{x_j}\rho}{2\ell'+3}\right)^{\ell'} \leq \frac{1}{3} \left(\frac{er_{x_j}\rho}{2\ell'+3}\right)^{\ell'}, \end{aligned}$$

where the first inequality follows from (66), [11, 10.14.4] and (70), the second inequality follows from [11, 5.6.1] and the final equality follows from the fact that

$$\frac{e^{3/2}}{4\sqrt{2\pi}} \frac{\sqrt{2\ell'+1}}{\ell'+3/2} \leq \frac{1}{3},$$

for non-negative integers ℓ' , with $\ell' = 1$ maximizing the left hand side. Using $|w_s| \leq \frac{8\pi}{S^2}$ from (85), it follows that

$$\begin{aligned} & \left| \sum_{s=0}^S \sum_{t=0}^{S-1} w_s Y_{\ell'}^{m'}(\gamma_s) \overline{Y_{\ell'}^m(\gamma_s)} - \int_{\mathbb{S}^2} Y_{\ell'}^{m'}(\gamma_\omega) \overline{Y_{\ell'}^m(\gamma_\omega)} d\sigma(\gamma_\omega) \right| \\ & \leq \sum_{s=0}^S \sum_{t=0}^{S-1} \frac{8\pi}{S^2} |Y_{\ell'}^{m'}(\gamma_s) \overline{Y_{\ell'}^m(\gamma_s)}| + \int_{\mathbb{S}^2} |Y_{\ell'}^{m'}(\gamma_\omega) \overline{Y_{\ell'}^m(\gamma_\omega)}| d\sigma(\gamma_\omega) \\ & \leq \frac{8\pi}{S^2} S(S+1) \sqrt{\frac{2\ell'+1}{4\pi}} \sqrt{\frac{2\ell+1}{4\pi}} + 4\pi \sqrt{\frac{2\ell'+1}{4\pi}} \sqrt{\frac{2\ell+1}{4\pi}} \\ & \leq \frac{112\pi}{9} \sqrt{\frac{2\ell'+1}{4\pi}} \sqrt{\frac{2\ell+1}{4\pi}}, \end{aligned}$$

where the second inequality used (70) and the third that $\frac{S(S+1)}{S^2} \leq \frac{19}{18}$ since $S \geq \lceil 2e\lambda_1 \rceil = \lceil 2e\lambda_{01} \rceil = 18$. Inserting this into (36) and using (37) results in

$$\begin{aligned} R_{\ell,m,j}(\rho) &= \left| \sum_{\ell'=\lfloor S/2 \rfloor + 1}^{\infty} \sum_{m'=-\ell'}^{\ell'} \frac{i^{\ell'}}{4\pi} \alpha_{m',\ell'} \left(\sum_{s=0}^S \sum_{t=0}^{S-1} w_s Y_{\ell'}^{m'}(\gamma_s) \overline{Y_{\ell'}^m(\gamma_s)} \right. \right. \\ & \quad \left. \left. - \int_{\mathbb{S}^2} Y_{\ell'}^{m'}(\gamma_\omega) \overline{Y_{\ell'}^m(\gamma_\omega)} d\sigma(\gamma_\omega) \right) \right| \\ & \leq \sum_{\ell'=\lfloor S/2 \rfloor + 1}^{\infty} \sum_{m'=-\ell'}^{\ell'} \left| \frac{i^{\ell'}}{4\pi} \alpha_{m',\ell'} \right| \frac{112\pi}{9} \sqrt{\frac{2\ell'+1}{4\pi}} \sqrt{\frac{2\ell+1}{4\pi}} \\ & \leq \sum_{\ell'=\lfloor S/2 \rfloor + 1}^{\infty} \sum_{m'=-\ell'}^{\ell'} \frac{112\pi}{27} \left(\frac{er_{x_j} \rho}{2\ell'+3} \right)^{\ell'} \sqrt{\frac{2\ell'+1}{4\pi}} \sqrt{\frac{2\ell+1}{4\pi}} \\ & = \frac{28}{27} \sqrt{2\ell+1} \sum_{\ell'=\lfloor S/2 \rfloor + 1}^{\infty} (2\ell'+1)^{3/2} \left(\frac{er_{x_j} \rho}{2\ell'+3} \right)^{\ell'} \\ & = \frac{28}{27} \sqrt{2\ell+1} (er_{x_j} \rho)^{3/2} \sum_{\ell'=\lfloor S/2 \rfloor + 1}^{\infty} \left(\frac{er_{x_j} \rho}{2\ell'+3} \right)^{\ell'-3/2} \\ & \leq \frac{28}{27} \sqrt{2\ell+1} (er_{x_j} \rho)^{3/2} \sum_{\ell'=\lfloor S/2 \rfloor + 1}^{\infty} \left(\frac{er_{x_j} \rho}{2(\lfloor S/2 \rfloor + 1) + 3} \right)^{\ell'-3/2}. \quad (38) \end{aligned}$$

Since we assume $S \geq 2er_{x_j} \rho$, it follows that $\frac{er_{x_j} \rho}{2(\lfloor S/2 \rfloor + 1) + 3} \leq 1/2$, so

$$\begin{aligned} R_{\ell,m,j} & \leq \frac{28}{27} \sqrt{2\ell+1} (er_{x_j} \rho)^{3/2} \sum_{\ell'=\lfloor S/2 \rfloor + 1}^{\infty} \left(\frac{1}{2} \right)^{\ell'-3/2} \\ & = \frac{28}{27} \sqrt{2\ell+1} (er_{x_j} \rho)^{3/2} \left(\frac{1}{2} \right)^{\lfloor S/2 \rfloor - 3/2} \\ & \leq \frac{28}{27} \sqrt{S+1} \left(\frac{S}{2} \right)^{3/2} \left(\frac{1}{2} \right)^{\lfloor S/2 \rfloor - 3/2} \leq 27.6 \cdot 2^{-S/4}, \end{aligned}$$

since

$$\frac{28}{27} \sqrt{S+1} \left(\frac{S}{2} \right)^{3/2} \left(\frac{1}{2} \right)^{\lfloor S/2 \rfloor - 3/2} 2^{S/4} \leq 27.6,$$

for integer S , where the left hand side is maximized at $S = 11$. Note that $r_{x_j} \leq 1$ and $\rho \leq \lambda_n$, and $L \leq \lambda_n$ by (24). Using (18), the conclusion then follows. \square

Remark 4.2 (Comparison to 2D angular node proof). The proof strategy for Lemma 4.2 is more significantly complicated than the analogous 2D result [39, Lemma 4.2]. When generalizing the 2D result, we noticed a gap in the 2D proof: the derivative estimate in the equation before [39, Eq. (4.2)] is not rigorously proven. In the present paper, we use a more complicated strategy, which avoids this issue. We remark that a similar approach can be used to rigorously establish [39, Lemma 4.2] up to a constant factor of 2.

Remark 4.3 (Optimizing the bound for S). The bounds used in the proof of Lemma 4.2 to show the asymptotic behavior of S are slightly conservative. In practice, we can numerically obtain smaller values of S through (38), by choosing the smallest integer S satisfying

$$\frac{28}{27} \sqrt{2\ell + 1} (e\lambda_n)^{3/2} \sum_{\ell'=\lfloor S/2 \rfloor + 1}^{\infty} \left(\frac{e\lambda_n}{2(\lfloor S/2 \rfloor + 1) + 3} \right)^{\ell' - 3/2} \leq \eta.$$

5. NUMERICAL EXPERIMENTS

This section applies Algorithms 1 and 2 to benchmarking problems. We first make two remarks on implementation details.

Remark 5.1. (Barycentric interpolation) There are many fast methods for performing the interpolation steps of Algorithms 1 and 2 [15, 22, 34, 14, 19, 41]. In practice, using precomputed sparse barycentric interpolation matrices [7] is simple, fast and accurate, and is therefore the method used in our implementation.

Remark 5.2. (FFT-based bandlimit heuristic) Previously, in §3.2, we derived the following upper bound on the bandlimit parameter:

$$\lambda = 6^{1/3} \pi^{2/3} \lfloor (N + 1)/2 \rfloor \approx 1.80N. \quad (39)$$

The main results of this paper guarantee that the operators B and B^* can be applied accurately and rapidly for any bandlimit bounded by λ . However, for applications that compute with the basis expansion operators B and B^* (e.g., in fast computations of least-squares problems involving these operators), using a slightly smaller bandlimit is necessary since the minimum singular values of B and B^* are very small at this value of λ . Determining the optimal practical bandlimit is a separate theoretical issue from fast computation and one not addressed here.

A heuristic that we find to be effective is based on the FFT. The maximum frequency of a centered FFT of length N is $\pi^2(N/2)^2$. Equating this frequency with the eigenvalue λ^2 gives

$$\lambda = \pi/2N \approx 1.57N. \quad (40)$$

Since this heuristic leads to a bandlimit less than (39), the accuracy guarantees of Theorem 3.1 apply. We use the bandlimit (40) for the numerical experiments below.

5.1. Accuracy. This section verifies the accuracy guarantees of Theorem 3.1. We compare the fast methods of Algorithms 1 and 2 to the dense method performed by explicitly forming and applying the matrix B from (6) with entries $B_{ij} = \psi_i(x_j)h^{3/2}$ and its adjoint B^* from (7), respectively. We denote the relative ℓ^1 - ℓ^∞ error comparing applications of B and B^* to their fast counterparts of Theorem 3.1 by

$$\text{err}_\alpha = \frac{\|B\alpha - \tilde{B}\alpha\|_{\ell^\infty}}{\|\alpha\|_{\ell^1}} \quad \text{and} \quad \text{err}_f = \frac{\|B^*f - \tilde{B}^*f\|_{\ell^\infty}}{\|f\|_{\ell^1}}. \quad (41)$$

TABLE 1. Relative accuracy of Algorithms 1 and 2.

N	ε	err_a	err_f	$\text{err}_{2,a}$	$\text{err}_{2,f}$
32	1.00000e-04	1.09147e-06	3.44431e-07	3.47059e-04	3.94597e-05
32	1.00000e-07	8.80468e-10	7.31137e-10	3.77298e-07	7.32120e-08
32	1.00000e-10	1.50301e-15	9.66415e-16	3.90013e-13	8.60492e-14
32	1.00000e-14	9.21641e-17	1.61313e-16	2.79836e-14	1.44868e-14
48	1.00000e-04	3.07614e-07	1.43754e-07	3.10650e-04	3.69283e-05
48	1.00000e-07	3.93735e-09	9.17106e-10	2.42870e-06	1.64956e-07
48	1.00000e-10	1.71840e-13	2.63019e-14	1.22662e-10	5.45878e-12
48	1.00000e-14	8.80011e-15	3.44285e-15	5.11352e-12	6.40179e-13
56	1.00000e-04	1.46292e-07	1.00198e-07	2.68961e-04	4.08369e-05
56	1.00000e-07	1.80844e-09	5.80538e-10	2.90177e-06	2.10560e-07
56	1.00000e-10	2.87442e-13	6.20621e-14	3.34660e-10	1.56999e-11
56	1.00000e-14	5.10866e-14	7.97114e-15	5.65145e-11	2.36787e-12

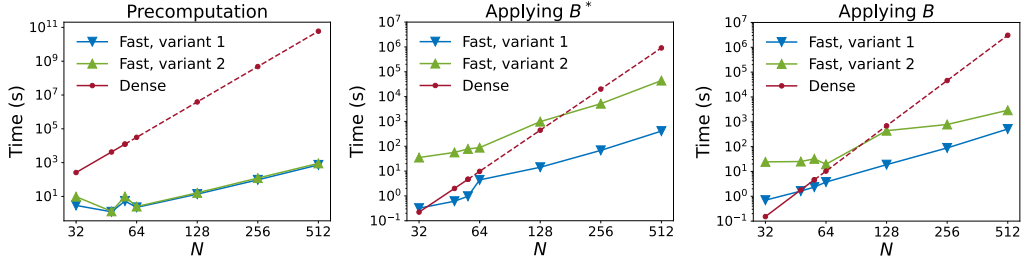


FIGURE 3. Timings of Algorithm 1 and Algorithm 2. “Variant 1” uses [8] for the fast spherical harmonics transform in steps 2 of Algorithm 1 and Algorithm 2, and “Variant 2” uses [51].

We verify that the Algorithms 1 and 2 achieve the $\ell^1 - \ell^\infty$ error guaranteed by Theorem 3.1. The experiments use as volume a 3D density map of the SARS-CoV-2 Omicron spike glycoprotein complex [24] downloaded from the online electron microscopy data bank [33] and illustrated in Figure 1. The computational results are shown in Table 1. Explicitly forming the dense matrices B becomes computationally prohibitive for moderate values of N and we can therefore only compute the dense operators up to $N = 56$. The experiments were performed on a machine with Intel Xeon E7-4870 processors and 1.5 TB of memory.

As an additional validation of the usefulness of Theorem 3.1, we also report the $\ell^2 - \ell^2$ errors

$$\text{err}_{2,\alpha} = \frac{\|B\alpha - \tilde{B}\alpha\|_{\ell^2}}{\|B\alpha\|_{\ell^2}} \quad \text{and} \quad \text{err}_{2,f} = \frac{\|B^*f - \tilde{B}^*f\|_{\ell^2}}{\|B^*f\|_{\ell^2}}. \quad (42)$$

The $\ell^1 - \ell^\infty$ errors are bounded by ε , as guaranteed by Theorem 3.1 and the $\ell^2 - \ell^2$ errors are close to ε , even though this is not a priori guaranteed by Theorem 3.1 given the hyperparameter settings chosen for the experiments.

5.2. Timings. This section verifies the computational complexity given in Theorem 3.1. We record the timings of the fast algorithms with two different choices of fast spherical harmonics transforms [8, 51]. The experiments used accuracy $\varepsilon = 10^{-7}$. The results are shown in Figure 3. We also show the time of each step of Algorithm 1 in Table 2.

TABLE 2. Timings of the steps of Algorithm 1. “Variant 1” uses [8] for the fast spherical harmonics transform in step 2 of Algorithm 1, and “Variant 2” uses [51]. The timings of Algorithm 2 are similar.

N	Variant 1			Variant 2		
	Step 1	Step 2	Step 3	Step 1	Step 2	Step 3
32	1.635e-01	1.470e-01	9.175e-03	2.935e-01	3.479e+01	9.008e-03
48	2.539e-01	3.326e-01	2.387e-02	4.938e-01	5.591e+01	1.962e-02
56	4.233e-01	5.082e-01	3.568e-02	7.001e-01	7.717e+01	3.043e-02
64	5.644e-01	3.799e+00	4.923e-02	1.272e+00	8.657e+01	4.251e-02
128	3.340e+00	1.058e+01	3.183e-01	7.637e+00	9.704e+02	2.682e-01
256	2.431e+01	4.142e+01	2.475e+00	5.365e+01	5.119e+03	1.830e+00
512	1.810e+02	2.016e+02	2.411e+01	4.178e+02	4.365e+04	1.920e+01

6. CONCLUSION

This paper developed fast methods to transform between a voxel representation of a three-dimensional function and its expansion into ball harmonics. We proved accuracy guarantees and demonstrated the performance of the methods in numerical experiments. To our knowledge, there are no existing transforms from a voxel representation of a 3D function into an analogous steerable basis that provide similar approximation with comparable time complexity and theoretical guarantees.

In future work, we plan to apply these fast ball harmonic transforms in pipelines for computationally demanding 3D data processing tasks, such as reconstruction algorithms in cryo-electron microscopy. It could also be interesting to adapt the approach here to other geometric domains, such as spherical annuli, which would involve identifying analytic analogues to the plane-wave expansion.

Acknowledgments. We thank Gregory Chirikjian and Jeremy Hoskins for their helpful comments on a draft of this paper. Some of this research was performed while authors JK, NFM, and AS were visiting the long program on Computational Microscopy (Fall 2022) at the Institute for Pure and Applied Mathematics, which is supported by NSF DMS 1925919. JK was supported in part by NSF DMS 2309782 and CISE-IIS 2312746, and start-up grants from the College of Natural Sciences and Oden Institute at UT Austin. NFM was supported in part by a start-up grant from Oregon State University. AS and OM were supported in part by AFOSR FA9550-20-1-0266 and FA9550-23-1-0249, the Simons Foundation Math+X Investigator Award, NSF DMS 2009753, and NIH/NIGMS R01GM136780-01.

REFERENCES

- [1] L. R. ABRAMO, P. H. REIMBERG, AND H. S. XAVIER, *CMB in a box: Causal structure and the Fourier-Bessel expansion*, Physical Review D, 82 (2010), p. 043510.
- [2] S. AKRAMUS SALEHIN AND T. D. ABHAYAPALA, *Frequency-radial duality based photoacoustic image reconstruction*, Journal of the Acoustical Society of America, 132 (2012), pp. 150–161.
- [3] A. S. BANERJEE, R. S. ELLIOTT, AND R. D. JAMES, *A spectral scheme for Kohn–Sham density functional theory of clusters*, Journal of Computational Physics, 287 (2015), pp. 226–253.
- [4] A. H. BARNETT, *Aliasing error of the $\exp(\beta\sqrt{1-z^2})$ kernel in the nonuniform fast Fourier transform*, Applied and Computational Harmonic Analysis, 51 (2021), pp. 1–16.
- [5] A. H. BARNETT, J. MAGLAND, AND L. AF KLINTEBERG, *A parallel nonuniform fast Fourier transform library based on an “Exponential of semicircle” kernel*, SIAM Journal on Scientific Computing, 41 (2019), pp. C479–C504.

- [6] T. BENDORY, Y. KHOO, J. KILEEL, O. MICKELIN, AND A. SINGER, *Autocorrelation analysis for cryo-EM with sparsity constraints: Improved sample complexity and projection-based algorithms*, Proceedings of the National Academy of Sciences, 120 (2023), p. e2216507120.
- [7] J.-P. BERRUT AND L. N. TREFETHEN, *Barycentric Lagrange interpolation*, SIAM Review, 46 (2004), pp. 501–517.
- [8] B. BONEV, T. KURTH, C. HUNDT, J. PATHAK, M. BAUST, K. KASHINATH, AND A. ANANDKUMAR, *Spherical Fourier neural operators: Learning stable dynamics on the sphere*, in International Conference on Machine Learning, PMLR, 2023, pp. 2806–2823.
- [9] N. BOULLÉ AND A. TOWNSEND, *Computing with functions in the ball*, SIAM Journal on Scientific Computing, 42 (2020), pp. C169–C191.
- [10] G. S. CHIRIKJIAN AND A. B. KYATKIN, *Harmonic Analysis for Engineers and Applied Scientists: Updated and Expanded Edition*, Courier Dover Publications, 2016.
- [11] *NIST Digital Library of Mathematical Functions*. <http://dlmf.nist.gov/>, Release 1.1.5 of 2022-03-15, <http://dlmf.nist.gov/>. Frank W. J. Olver, Adri B. Olde Daalhuis, Daniel W. Lozier, Barry I. Schneider, Ronald F. Boisvert, Charles W. Clark, Bruce R. Miller, Bonita V. Saunders, Howard S. Cohl, and Marjorie A. McClain, eds.
- [12] J. J. DONATELLI, P. H. ZWART, AND J. A. SETHIAN, *Iterative phasing for fluctuation X-ray scattering*, Proceedings of the National Academy of Sciences, 112 (2015), pp. 10286–10291.
- [13] J. R. DRISCOLL AND D. M. HEALY, *Computing Fourier transforms and convolutions on the 2-sphere*, Advances in Applied Mathematics, 15 (1994), pp. 202–250.
- [14] A. DUTT, M. GU, AND V. ROKHLIN, *Fast algorithms for polynomial interpolation, integration, and differentiation*, SIAM Journal on Numerical Analysis, 33 (1996), pp. 1689–1711, <https://doi.org/10.1137/0733082>.
- [15] A. DUTT AND V. ROKHLIN, *Fast Fourier transforms for nonequispaced data*, SIAM Journal on Scientific Computing, 14 (1993), pp. 1368–1393.
- [16] A. ELBERT, *Some recent results on the zeros of Bessel functions and orthogonal polynomials*, Journal of Computational and Applied Mathematics, 133 (2001), pp. 65–83.
- [17] V. L. GALINSKY AND L. R. FRANK, *Automated segmentation and shape characterization of volumetric data*, NeuroImage, 92 (2014), pp. 156–168.
- [18] J. GASTEIGER, J. GROSS, AND S. GÜNNEMANN, *Directional message passing for molecular graphs*, arXiv preprint arXiv:2003.03123, (2020).
- [19] Z. GIMBUTAS, N. F. MARSHALL, AND V. ROKHLIN, *A fast simple algorithm for computing the potential of charges on a line*, Applied and Computational Harmonic Analysis, 49 (2020), pp. 815–830.
- [20] T. D. GODDARD, C. C. HUANG, E. C. MENG, E. F. PETTERSEN, G. S. COUCH, J. H. MORRIS, AND T. E. FERRIN, *UCSF ChimeraX: Meeting modern challenges in visualization and analysis*, Protein Science, 27 (2018), pp. 14–25.
- [21] D. S. GREBENKOV AND B.-T. NGUYEN, *Geometrical structure of Laplacian eigenfunctions*, SIAM Review, 55 (2013), pp. 601–667, <https://doi.org/10.1137/120880173>.
- [22] L. GREENGARD AND J.-Y. LEE, *Accelerating the nonuniform fast Fourier transform*, SIAM Review, 46 (2004), pp. 443–454.
- [23] N. A. GUMEROV AND R. DURAISWAMI, *A broadband fast multipole accelerated boundary element method for the three dimensional Helmholtz equation*, Journal of the Acoustical Society of America, 125 (2009), pp. 191–205.
- [24] H. GUO, Y. GAO, T. LI, T. LI, Y. LU, L. ZHENG, Y. LIU, T. YANG, F. LUO, S. SONG, ET AL., *Structures of Omicron spike complexes and implications for neutralizing antibody development*, Cell Reports, 39 (2022), p. 110770.
- [25] J. GUO, *A note on the Weyl formula for balls in \mathbb{R}^d* , Proceedings of the American Mathematical Society, 149 (2021), pp. 1663–1675.
- [26] D. R. HEATH-BROWN, *Lattice points in the sphere*, Number Theory in Progress, 2 (1999), pp. 883–892.
- [27] R. HOLLERBACH, *A spectral solution of the magneto-convection equations in spherical geometry*, International Journal for Numerical Methods in Fluids, 32 (2000), pp. 773–797.
- [28] Z. KAM, *The reconstruction of structure from electron micrographs of randomly oriented particles*, Journal of Theoretical Biology, 82 (1980), pp. 15–39.
- [29] J. KEINER, S. KUNIS, AND D. POTTS, *Using NFFT 3—A software library for various nonequispaced fast Fourier transforms*, ACM Transactions on Mathematical Software (TOMS), 36 (2009), pp. 1–30.
- [30] J. KEINER AND D. POTTS, *Fast evaluation of quadrature formulae on the sphere*, Mathematics of Computation, 77 (2008), pp. 397–419.

- [31] J. A. KOVACS AND W. WRIGGERS, *Fast rotational matching*, Acta Crystallographica Section D: Biological Crystallography, 58 (2002), pp. 1282–1286.
- [32] F. LANUSSE, A. RASSAT, AND J.-L. STARCK, *Spherical 3D isotropic wavelets*, Astronomy & Astrophysics, 540 (2012), p. A92.
- [33] C. L. LAWSON, A. PATWARDHAN, M. L. BAKER, C. HRYC, E. S. GARCIA, B. P. HUDSON, I. LAGERSTEDT, S. J. LUDTKE, G. PINTILIE, R. SALA, ET AL., *EMDataBank unified data resource for 3DEM*, Nucleic Acids Research, 44 (2016), pp. D396–D403.
- [34] J.-Y. LEE AND L. GREENGARD, *The type 3 nonuniform FFT and its applications*, Journal of Computational Physics, 206 (2005), pp. 1–5.
- [35] B. LEISTEDT AND J. D. MCEWEN, *Exact wavelets on the ball*, IEEE Transactions on Signal Processing, 60 (2012), pp. 6257–6269.
- [36] B. LEISTEDT, H. V. PEIRIS, AND J. D. MCEWEN, *Flaglets for studying the large-scale structure of the Universe*, in Wavelets and Sparsity XV, vol. 8858, SPIE, 2013, pp. 130–142.
- [37] B. LEISTEDT, A. RASSAT, A. REFREGIER, AND J.-L. STARCK, *3DEX: A code for fast spherical Fourier-Bessel decomposition of 3D surveys*, Astronomy & Astrophysics, 540 (2012), p. A60.
- [38] W. LOWRIE AND A. FICHTNER, *Fundamentals of Geophysics*, Cambridge University Press, 2020.
- [39] N. F. MARSHALL, O. MICKELIN, AND A. SINGER, *Fast expansion into harmonics on the disk: A steerable basis with fast radial convolutions*, SIAM Journal on Scientific Computing, 45 (2023), pp. A2431–A2457, <https://doi.org/10.1137/22M1542775>.
- [40] J. D. MCEWEN AND B. LEISTEDT, *Fourier-Laguerre transform, convolution and wavelets on the ball*, arXiv preprint arXiv:1307.1307, (2013).
- [41] G. PLONKA, D. POTTS, G. STEIDL, AND M. TASCHE, *Numerical Fourier Analysis*, Springer, 2018.
- [42] A. POLITIS, M. R. P. THOMAS, H. GAMPER, AND I. J. TASHEV, *Applications of 3D spherical transforms to personalization of head-related transfer functions*, in 2016 IEEE International Conference on Acoustics, Speech and Signal Processing (ICASSP), IEEE, 2016, pp. 306–310.
- [43] D. POTTS AND G. STEIDL, *Fast summation at nonequispaced knots by NFFT*, SIAM Journal on Scientific Computing, 24 (2003), pp. 2013–2037.
- [44] D. POTTS, G. STEIDL, AND M. TASCHE, *Fast and stable algorithms for discrete spherical Fourier transforms*, Linear Algebra and its Applications, 275 (1998), pp. 433–450.
- [45] A. RASSAT AND A. REFREGIER, *3D spherical analysis of baryon acoustic oscillations*, Astronomy & Astrophysics, 540 (2012), p. A115.
- [46] H. ROBBINS, *A remark on Stirling’s formula*, The American Mathematical Monthly, 62 (1955), pp. 26–29.
- [47] V. ROKHLIN, *A fast algorithm for the discrete Laplace transformation*, Journal of Complexity, 4 (1988), pp. 12–32, [https://doi.org/https://doi.org/10.1016/0885-064X\(88\)90007-6](https://doi.org/https://doi.org/10.1016/0885-064X(88)90007-6), <https://www.sciencedirect.com/science/article/pii/0885064X88900076>.
- [48] V. ROKHLIN AND M. TYGERT, *Fast Algorithms for Spherical Harmonic Expansions*, SIAM J. Sci. Comput., 27 (2006), pp. 1903–1928, <https://doi.org/10.1137/050623073>.
- [49] S. A. SALEHIN AND T. D. ABHAYAPALA, *Photoacoustic image reconstruction from a frequency-invariant source localization perspective*, in 2010 18th European Signal Processing Conference, IEEE, 2010, pp. 1627–1631.
- [50] N. SHARON, J. KILEEL, Y. KHOO, B. LANDA, AND A. SINGER, *Method of moments for 3D single particle ab initio modeling with non-uniform distribution of viewing angles*, Inverse Problems, 36 (2020), p. 044003.
- [51] R. M. SLEVINSKY, *Fast and backward stable transforms between spherical harmonic expansions and bivariate Fourier series*, Applied and Computational Harmonic Analysis, 47 (2019), pp. 585–606.
- [52] E. M. STEIN AND G. WEISS, *Introduction to Fourier Analysis on Euclidean Spaces*, vol. 1, Princeton University Press, 1971.
- [53] J. WALDVOGEL, *Fast construction of the Fejér and Clenshaw–Curtis quadrature rules*, BIT Numerical Mathematics, 46 (2006), pp. 195–202.
- [54] Q. WANG, O. RONNEBERGER, AND H. BURKHARDT, *Rotational invariance based on Fourier analysis in polar and spherical coordinates*, IEEE Transactions on Pattern Analysis and Machine Intelligence, 31 (2009), pp. 1715–1722.
- [55] C. WÜLKER, *Fast SGL Fourier transforms for scattered data*, Applied and Computational Harmonic Analysis, 49 (2020), pp. 1107–1135.

APPENDIX A. PROOF OF THEOREM 3.1

The proof of Theorem 3.1 is divided into Claims A.1 and A.2, which establish the accuracy guarantee for Algorithm 1 and 2, respectively, followed by Claim A.3 which

establishes the computational complexity for both algorithms. These results rely on technical lemmas established in §A.4.

A.1. Accuracy bounds for Algorithm 1.

Claim A.1. *Assume $\lambda \leq 6^{1/3}\pi^{2/3}\lfloor(V^{1/3} + 1)/2\rfloor$ and $\varepsilon > 0$ is a user-specified accuracy parameter satisfying $|\log_2 \varepsilon| \leq 5.3V^{1/3}$. Then Algorithm 1 produces output \tilde{B}^*f satisfying*

$$\|\tilde{B}^*f - B^*f\|_{\ell^\infty} \leq \varepsilon\|f\|_{\ell^1},$$

for all inputs f .

Proof of Claim A.1. In this step, we will use the observation

$$\sum_{s=0}^S \sum_{t=0}^{S-1} w_s = 4\pi, \quad (43)$$

which follows from the exactness of the quadrature rule (84) and the fact that $Y_0^0(\gamma)$ is a constant function. We will also use the observation

$$\begin{aligned} \sum_{s=0}^S \sum_{t=0}^{S-1} |w_s \overline{Y_{\ell_i}^{m_i}(\gamma_{s,t})}| &\leq \left(\sum_{s=0}^S \sum_{t=0}^{S-1} Y_{\ell_i}^{m_i}(\gamma_{s,t}) \overline{Y_{\ell_i}^{m_i}(\gamma_{s,t})} w_s \right)^{1/2} \left(\sum_{s=0}^S \sum_{t=0}^{S-1} w_s \right)^{1/2} \\ &= \sqrt{4\pi}, \end{aligned} \quad (44)$$

which follows from Cauchy-Schwarz, the fact that $w_s \geq 0$ from (86) and exactness of the quadrature rule (84).

Denote $\alpha = \tilde{B}^*f$. By writing out the results of the steps of the algorithm and including the error terms induced by the fast and approximate applications of the NUFFT, spherical harmonics transform, and the interpolation steps, respectively, we have

$$\begin{aligned} \alpha_i = c_i h^{3/2} &\left(\sum_{q=0}^{Q-1} \left(\frac{\lambda_i}{4\pi} \left(\sum_{s=0}^S \sum_{t=0}^{S-1} \left(\sum_{j=1}^V f_j e^{-ix_j \cdot \rho_q \gamma_{s,t}} + \delta_{qst}^{\text{nuft}} \right) \right. \right. \right. \\ &\left. \left. \left. \times w_s \overline{Y_{\ell_i}^{m_i}(\gamma_{s,t})} \right) + \delta_q^{\text{fsh}} \right) u_q(\lambda_i) + \delta_i^{\text{in}} \right), \end{aligned}$$

where $\delta_{qst}^{\text{nuft}}$, δ_q^{fsh} and δ_i^{in} denote the error from the NUFFT, spherical harmonics transform, and fast interpolation, respectively. We will also denote by $\varepsilon^{\text{nuft}}$, ε^{fsh} and ε^{in} the relative error parameters for the NUFFT, fast spherical harmonic transform, and fast interpolation, respectively. The error induced by the fast application of the NUFFT satisfies the ℓ^1 - ℓ^∞ relative error bound [4, 5]

$$\|\delta^{\text{nuft}}\|_{\ell^\infty} \leq \varepsilon^{\text{nuft}} \sum_{j=1}^V |f_j e^{-ix_j \cdot \rho_q \gamma_{s,t}}| = \varepsilon^{\text{nuft}} \|f\|_{\ell^1}. \quad (45)$$

Next, assume $\varepsilon^{\text{nuft}} \leq 1$ (which we will ensure holds below), which together with (85) shows that the error of the fast spherical harmonics step satisfies the $\ell^1 - \ell^\infty$ error bound [30, 29]

$$\begin{aligned} \|\delta^{\text{fsh}}\|_{\ell^\infty} &\leq \frac{\varepsilon^{\text{fsh}}}{4\pi} \sum_{s=0}^S \sum_{t=0}^{S-1} \left| w_s \left(\sum_{j=1}^V f_j e^{-ix_j \cdot \rho_q \gamma_{s,t}} + \delta_{qst}^{\text{nuft}} \right) \right| \\ &\leq \frac{\varepsilon^{\text{fsh}}}{4\pi} \sum_{s=0}^S \sum_{t=0}^{S-1} w_s (1 + \varepsilon^{\text{nuft}}) \|f\|_{\ell^1} \leq 2\varepsilon^{\text{fsh}} \|f\|_{\ell^1}. \end{aligned} \quad (46)$$

where the last inequality used (43), (86) and that $\varepsilon^{\text{nuf}} \leq 1$. Assuming $Q\varepsilon^{\text{in}} \leq 1$ (which we will choose to hold below), the error of the fast interpolation step satisfies (see [14] also see §A.3 for further discussion of fast interpolation methods)

$$\begin{aligned} \|\delta^{\text{in}}\|_{\ell^\infty} &\leq \varepsilon^{\text{in}} \sum_{q=0}^{Q-1} \left| \frac{\iota^{\ell_i}}{4\pi} \sum_{s=0}^S \sum_{t=0}^{S-1} \left(\sum_{j=1}^V f_j e^{-ix_j \cdot \rho_q \gamma_{s,t}} + \delta_{qst}^{\text{nuf}} \right) w_s \overline{Y_{\ell_i}^{m_i}(\gamma_{s,t})} + \delta_q^{\text{fsh}} \right| \\ &\leq \varepsilon^{\text{in}} \sum_{q=0}^{Q-1} \left(\frac{1}{4\pi} \sum_{s=0}^S \sum_{t=0}^{S-1} (1 + \varepsilon^{\text{nuf}}) \|f\|_{\ell^1} \left| w_s \overline{Y_{\ell_i}^{m_i}(\gamma_{s,t})} \right| + \delta_q^{\text{fsh}} \right) \\ &\leq \varepsilon^{\text{in}} Q \|f\|_{\ell^1} + 2\varepsilon^{\text{in}} \varepsilon^{\text{fsh}} Q \|f\|_{\ell^1} \leq \varepsilon^{\text{in}} Q \|f\|_{\ell^1} + 2\varepsilon^{\text{fsh}} \|f\|_{\ell^1}. \end{aligned} \quad (47)$$

Note that the third inequality in (47) used (44).

Next, denote by α'_i the result of applying Algorithm 1 without the error induced by the approximations in the NUFFT, spherical harmonics transform and fast interpolation steps, i.e.,

$$\alpha'_i = c_i h^{3/2} \frac{\iota^{\ell_i}}{4\pi} \sum_{q=0}^{Q-1} \sum_{s=0}^S \sum_{t=0}^{S-1} \sum_{j=1}^V f_j e^{-ix_j \cdot \rho_q \gamma_{s,t}} w_s \overline{Y_{\ell_i}^{m_i}(\gamma_{s,t})} u_q(\lambda_i). \quad (48)$$

This results in

$$\begin{aligned} |\alpha_i - \alpha'_i| &\leq c_i h^{3/2} \left(\sum_{q=0}^{Q-1} \left(\frac{1}{4\pi} \|\delta^{\text{nuf}}\|_{\ell^\infty} \left(\sum_{s=0}^S \sum_{t=0}^{S-1} w_s |Y_{\ell_i}^m(\gamma_{s,t})| \right) + \|\delta^{\text{fsh}}\|_{\ell^\infty} \right) \right. \\ &\quad \left. \times u_q(\lambda_i) + \|\delta^{\text{in}}\|_{\ell^\infty} \right) \\ &\leq c_i h^{3/2} \left(\left(\frac{1}{2\sqrt{\pi}} \|\delta^{\text{nuf}}\|_{\ell^\infty} + \|\delta^{\text{fsh}}\|_{\ell^\infty} \right) \sum_{q=0}^{Q-1} |u_q(\lambda_i)| + \|\delta^{\text{in}}\|_{\ell^\infty} \right) \\ &\leq \pi^2 (3/2)^{1/4} \left(\left(\frac{\|\delta^{\text{nuf}}\|_{\ell^\infty}}{2\sqrt{\pi}} + \|\delta^{\text{fsh}}\|_{\ell^\infty} \right) \left(2 + \frac{\pi}{2} \log Q \right) + \|\delta^{\text{in}}\|_{\ell^\infty} \right), \end{aligned} \quad (49)$$

where the last inequality used $\sum_{q=0}^{Q-1} |u_q(\lambda_i)| \leq (2 + \frac{\pi}{2} \log Q)$ (see [47, Eq. (11)]) and $c_i h^{3/2} \leq \pi^2 (3/2)^{1/4}$, from Lemma A.2. Combining this inequality with (45), (46) and (47) gives

$$\|\alpha - \alpha'\|_{\ell^\infty} \leq \pi^2 \left(\frac{3}{2} \right)^{1/4} \left(\left(\frac{\varepsilon^{\text{nuf}}}{2\sqrt{\pi}} + 2\varepsilon^{\text{fsh}} \right) \left(2 + \frac{\pi}{2} \log Q \right) + Q\varepsilon^{\text{in}} + 2\varepsilon^{\text{fsh}} \right) \|f\|_{\ell^1}.$$

Choosing the parameters

$$\varepsilon^{\text{nuf}} = \frac{\varepsilon / (2\pi^{3/2} (3/2)^{1/4})}{(2 + \frac{\pi}{2} \log Q)}, \quad \varepsilon^{\text{in}} = \frac{\varepsilon / (4\pi^2 (3/2)^{1/4})}{Q}, \quad \varepsilon^{\text{fsh}} = \frac{\varepsilon / (8\pi^2 (3/2)^{1/4})}{3 + \frac{\pi}{2} \log Q} \quad (50)$$

therefore results in

$$\|\alpha - \alpha'\|_{\ell^\infty} \leq \frac{3\varepsilon}{4} \|f\|_{\ell^1}. \quad (51)$$

We lastly relate α'_i to $(B^* f)_i$. The definition (48) gives

$$\begin{aligned} \alpha'_i &= c_i h^{3/2} \frac{\iota^{\ell_i}}{4\pi} \sum_{q=0}^{Q-1} \sum_{s=0}^S \sum_{t=0}^{S-1} \sum_{j=1}^V f_j e^{-ix_j \cdot \rho_q \gamma_{s,t}} w_s \overline{Y_{\ell_i}^{m_i}(\gamma_{s,t})} u_q(\lambda_i) \\ &= c_i h^{3/2} \sum_{j=1}^V f_j \left(j_{\ell_i}(r_j \lambda_i) \overline{Y_{\ell_i}^{m_i}(\gamma_{x_j})} + \delta_{i,j}^{\text{dis}} \right) = (B^* f)_i + c_i h^{3/2} \sum_{j=1}^V f_j \delta_{i,j}^{\text{dis}}, \end{aligned} \quad (52)$$

where the second equality follows from Lemma A.1 and $\delta_{i,j}^{\text{dis}}$ is a discretization error that satisfies $\|\delta^{\text{dis}}\|_{\ell^\infty} \leq (3 + \frac{\pi}{2} \log Q) \varepsilon^{\text{dis}}$. This results in

$$|\alpha'_i - (B^* f)_i| \leq c_i h^{3/2} \|f\|_{\ell^1} \|\delta^{\text{dis}}\|_{\ell^\infty} \leq \pi^2 (3/2)^{1/4} (3 + \frac{\pi}{2} \log Q) \varepsilon^{\text{dis}} \|f\|_{\ell^1}. \quad (53)$$

Set

$$\varepsilon^{\text{dis}} = \left(\pi^2 (3/2)^{1/4} \left(3 + \frac{\pi}{2} \log \left[5.3V^{1/3} \right] \right) \right)^{-1} \frac{\varepsilon}{4}. \quad (54)$$

Note that $\varepsilon^{\text{dis}} \leq \varepsilon$ so the assumption $5.3V^{1/3} \geq |\log_2 \varepsilon|$ then implies

$$Q = \log \lceil \max\{5.3V^{1/3}, \log_2 \varepsilon^{\text{dis}}\} \rceil = \log \lceil 5.3V^{1/3} \rceil.$$

Combining (53) and (51) then gives $\|\alpha - B^* f\|_{\ell^\infty} = \|\tilde{B}^* f - B^* f\|_{\ell^\infty} \leq \varepsilon \|f\|_{\ell^1}$. \square

A.2. Accuracy bounds for Algorithm 2.

Claim A.2. *Assume $\lambda \leq 6^{1/3} \pi^{2/3} \lfloor (V^{1/3} + 1)/2 \rfloor$ and $\varepsilon > 0$ is a user-specified accuracy parameter satisfying $|\log_2 \varepsilon| \leq 5.3V^{1/3}$. Then Algorithm 2 produces output $\tilde{B}\alpha$ that satisfies the accuracy bounds*

$$\|\tilde{B}\alpha - B\alpha\|_{\ell^\infty} \leq \varepsilon \|\alpha\|_{\ell^1},$$

for all inputs α .

Proof of Claim A.2. Denote $f = \tilde{B}\alpha$. By writing out the results of the steps of the algorithm and including the error terms induced by the fast and approximate applications of the interpolation step, the spherical harmonics transform and the NUFFT, respectively, we have

$$f_j = \sum_{q=0}^{Q-1} \left(\sum_{s=0}^S \sum_{t=0}^{S-1} \left(\sum_{\ell=0}^L \sum_{m=-\ell}^{\ell} \left(\sum_{\substack{i:\ell_i=\ell, \\ m_i=m}} c_i \alpha_i u_q(\lambda_i) h^{3/2} + \delta_{q,\ell,m}^{\text{in}} \right) \times \frac{(-t)^\ell}{4\pi} w_s Y_\ell^m(\gamma_{s,t}) \right) + \delta_{qst}^{\text{fsh}} \right) e^{ix_j \cdot \rho_q \gamma_{s,t}} + \delta_j^{\text{nuf}},$$

where $\delta_{q,\ell,m}^{\text{in}}$, $\delta_{q,s,t}^{\text{fsh}}$, δ_j^{nuf} denote the error from the fast interpolation, fast spherical harmonics transform and NUFFT, respectively. We will also denote by ε^{in} , ε^{fsh} and ε^{nuf} the relative error parameters for the fast interpolation, fast spherical harmonic transform and NUFFT, respectively. The error induced by the fast interpolation satisfies the ℓ^1 - ℓ^∞ relative error bound (see [14] and see also §A.3 for further discussion of fast interpolation methods) so

$$\|\delta_{\ell,m}^{\text{in}}\|_{\ell^\infty} \leq \varepsilon^{\text{in}} \sum_{\substack{i:\ell_i=\ell, \\ m_i=m}} c_i h^{3/2} |\alpha_i| \leq \pi^2 (3/2)^{1/4} \varepsilon^{\text{in}} \sum_{\substack{i:\ell_i=\ell, \\ m_i=m}} |\alpha_i|, \quad (55)$$

where $\delta_{\ell,m}^{\text{in}}$ is the vector defined by $\delta_{\ell,m}^{\text{in}} = (\delta_{q,\ell,m}^{\text{in}})_{q=0}^{Q-1}$. It follows that

$$\sum_{\ell=0}^L \sum_{m=-\ell}^{\ell} \|\delta_{\ell,m}^{\text{in}}\|_{\ell^\infty} \leq \pi^2 (3/2)^{1/4} \varepsilon^{\text{in}} \|\alpha\|_{\ell^1}.$$

Furthermore, the fast spherical harmonics error [30, 29] satisfies

$$\|\delta_{s,t}^{\text{fsh}}\|_{\ell^\infty} \leq \varepsilon^{\text{fsh}} \left| \sum_{\ell=0}^L \sum_{m=-\ell}^{\ell} \left(\sum_{\substack{i:\ell_i=\ell, \\ m_i=m}} c_i \alpha_i u_q(\lambda_i) h^{3/2} + \delta_{q,\ell,m}^{\text{in}} \right) \frac{(-t)^\ell}{4\pi} w_s \right|$$

$$\begin{aligned}
&\leq \frac{\varepsilon^{\text{fsh}}}{4\pi} \sum_{i=1}^n |c_i \alpha_i u_q(\lambda_i) h^{3/2} w_s| + \frac{\varepsilon^{\text{fsh}}}{4\pi} \sum_{\ell=0}^L \sum_{m=-\ell}^{\ell} |\delta_{\ell,m}^{\text{in}} w_s| \\
&\leq \frac{\varepsilon^{\text{fsh}}}{4\pi} \pi^2 (3/2)^{1/4} w_s \sum_{i=1}^n |u_q(\lambda_i) \alpha_i| + \varepsilon^{\text{in}} \frac{\varepsilon^{\text{fsh}}}{4\pi} \|\alpha\|_{\ell^1} \pi^2 (3/2)^{1/4} w_s,
\end{aligned}$$

where the third inequality used Lemma A.2, [39, Lemma A.2], (85) and (55). Using (43), it follows that

$$\sum_{s=0}^S \sum_{t=0}^{S-1} \|\delta_{s,t}^{\text{fsh}}\|_{\ell^\infty} \leq \varepsilon^{\text{fsh}} \pi^2 (3/2)^{1/4} \sum_{i=1}^n |u_q(\lambda_i) \alpha_i| + \varepsilon^{\text{in}} \varepsilon^{\text{fsh}} \|\alpha\|_{\ell^1} \pi^2 (3/2)^{1/4}.$$

Lastly, the error for the NUFFT [4, 5] satisfies

$$\begin{aligned}
\|\delta^{\text{nuf}}\|_{\ell^\infty} &\leq \varepsilon^{\text{nuf}} \left(\sum_{q=0}^{Q-1} \sum_{s=0}^S \sum_{t=0}^{S-1} \left(\sum_{\ell=0}^L \sum_{m=-\ell}^{\ell} \left(\sum_{\substack{i:\ell_i=\ell, \\ m_i=m}} |c_i \alpha_i u_q(\lambda_i) h^{3/2}| + |\delta_{q,\ell,m}^{\text{in}}| \right) \right. \right. \\
&\quad \left. \left. \times \frac{1}{4\pi} |w_s Y_\ell^m(\gamma_{s,t})| \right) + |\delta_{qst}^{\text{fsh}}| \right) \\
&\leq \frac{\varepsilon^{\text{nuf}}}{\sqrt{4\pi}} \sum_{q=0}^{Q-1} \sum_{\ell=0}^L \left(\sum_{m=-\ell}^{\ell} \left(\sum_{\substack{i:\ell_i=\ell, \\ m_i=m}} c_i |\alpha_i u_q(\lambda_i)| h^{3/2} + |\delta_{q,\ell,m}^{\text{in}}| \right) \right) \\
&\quad + \varepsilon^{\text{nuf}} \sum_{q=0}^{Q-1} \sum_{s=0}^S \sum_{t=0}^{S-1} |\delta_{qst}^{\text{fsh}}| \\
&\leq \frac{\varepsilon^{\text{nuf}}}{\sqrt{4\pi}} \left(\sum_{i=1}^n \left(\sum_{q=0}^{Q-1} |u_q(\lambda_i)| \right) c_i h^{3/2} |\alpha_i| + \sum_{q=0}^{Q-1} \pi^2 (3/2)^{1/4} \varepsilon^{\text{in}} \|\alpha\|_{\ell^1} \right) \\
&\quad + \varepsilon^{\text{nuf}} \sum_{q=0}^{Q-1} \left(\varepsilon^{\text{fsh}} \pi^2 (3/2)^{1/4} \sum_{i=1}^n |u_q(\lambda_i) \alpha_i| + \varepsilon^{\text{in}} \varepsilon^{\text{fsh}} \|\alpha\|_{\ell^1} \pi^2 (3/2)^{1/4} \right) \\
&\leq \frac{\varepsilon^{\text{nuf}}}{\sqrt{4\pi}} \left(\left(2 + \frac{\pi}{2} \log Q \right) \pi^2 (3/2)^{1/4} \|\alpha\|_{\ell^1} + Q \pi^2 (3/2)^{1/4} \varepsilon^{\text{in}} \|\alpha\|_{\ell^1} \right) \\
&\quad + \varepsilon^{\text{nuf}} \left(\varepsilon^{\text{fsh}} \pi^2 (3/2)^{1/4} \left(2 + \frac{\pi}{2} \log Q \right) \|\alpha\|_{\ell^1} + Q \varepsilon^{\text{in}} \varepsilon^{\text{fsh}} \|\alpha\|_{\ell^1} \pi^2 (3/2)^{1/4} \right) \\
&\leq \frac{\varepsilon^{\text{nuf}}}{\sqrt{4\pi}} \pi^2 (3/2)^{1/4} \left(\left(2 + \frac{\pi}{2} \log Q \right) + 1 \right) \left(1 + \varepsilon^{\text{fsh}} \sqrt{4\pi} \right) \|\alpha\|_{\ell^1},
\end{aligned}$$

where the second equality uses (44), the fourth uses [47, Eq. (11)] and the fifth assumes $Q \varepsilon^{\text{in}} \leq 1$, which we will show holds below.

Next, denote by \tilde{f} the result of applying Algorithm 2 without the error induced by the approximations in the fast interpolation, spherical harmonics transform and NUFFT steps, i.e.,

$$f'_j = \sum_{q=0}^{Q-1} \sum_{s=0}^S \sum_{t=0}^{S-1} \sum_{\ell=0}^L \sum_{m=-\ell}^{\ell} \sum_{\substack{i:\ell_i=\ell, \\ m_i=m}} c_i \alpha_i u_q(\lambda_i) h^{3/2} \frac{(-i)^\ell}{4\pi} w_s Y_\ell^m(\gamma_{s,t}) e^{i x_j \cdot \rho_q \gamma_{s,t}}. \quad (56)$$

We have

$$|f_j - f'_j| \leq \left(\sum_{q=0}^{Q-1} \sum_{s=0}^S \sum_{t=0}^{S-1} \left(\sum_{\ell=0}^L \sum_{m=-\ell}^{\ell} \|\delta_{\ell,m}^{\text{in}}\|_{\ell^\infty} \frac{1}{4\pi} |w_s Y_\ell^m(\gamma_{s,t})| \right) + |\delta_{qst}^{\text{fsh}}| \right) + |\delta_j^{\text{nuf}}|$$

$$\begin{aligned}
&\leq \frac{1}{\sqrt{4\pi}} \left(\sum_{q=0}^{Q-1} \pi^2 (3/2)^{1/4} \varepsilon^{\text{in}} \|\alpha\|_{\ell^1} \right) \\
&\quad + \sum_{q=0}^{Q-1} \left(\varepsilon^{\text{fsh}} \pi^2 (3/2)^{1/4} \sum_{i=1}^n |u_q(\lambda_i) \alpha_i| + \varepsilon^{\text{in}} \varepsilon^{\text{fsh}} \|\alpha\|_{\ell^1} \pi^2 (3/2)^{1/4} \right) \\
&\quad + \frac{\varepsilon^{\text{nuf}}}{\sqrt{4\pi}} \pi^2 (3/2)^{1/4} \left(\left(2 + \frac{\pi}{2} \log Q\right) + 1 \right) \left(1 + \varepsilon^{\text{fsh}} \sqrt{4\pi}\right) \|\alpha\|_{\ell^1} \\
&\leq \frac{1}{\sqrt{4\pi}} Q \pi^2 (3/2)^{1/4} \varepsilon^{\text{in}} \|\alpha\|_{\ell^1} \\
&\quad + \varepsilon^{\text{fsh}} \pi^2 (3/2)^{1/4} \left(2 + \frac{\pi}{2} \log Q\right) \|\alpha\|_{\ell^1} + Q \varepsilon^{\text{in}} \varepsilon^{\text{fsh}} \|\alpha\|_{\ell^1} \pi^2 (3/2)^{1/4} \\
&\quad + \frac{\varepsilon^{\text{nuf}}}{\sqrt{4\pi}} \pi^2 (3/2)^{1/4} \left(\left(2 + \frac{\pi}{2} \log Q\right) + 1 \right) \left(1 + \varepsilon^{\text{fsh}} \sqrt{4\pi}\right) \|\alpha\|_{\ell^1} \\
&\leq \pi^2 (3/2)^{1/4} \left(\frac{\varepsilon^{\text{in}} Q}{\sqrt{4\pi}} + \varepsilon^{\text{fsh}} \left(3 + \frac{\pi}{2} \log Q\right) + \frac{2\varepsilon^{\text{nuf}}}{\sqrt{4\pi}} \left(3 + \frac{\pi}{2} \log Q\right) \right) \|\alpha\|_{\ell^1},
\end{aligned}$$

where the last equation used $Q\varepsilon^{\text{in}} \leq 1$ and $\sqrt{4\pi}\varepsilon^{\text{in}} \leq 1$, which we will show holds below. Choosing the parameters

$$\varepsilon^{\text{in}} = \frac{1}{4Q} \frac{2\sqrt{\pi}\varepsilon}{\pi^2 (3/2)^{1/4}}, \quad \varepsilon^{\text{fsh}} = \frac{1}{4} \frac{\varepsilon / (\pi^2 (3/2)^{1/4})}{3 + \frac{\pi}{2} \log Q}, \quad \varepsilon^{\text{nuf}} = \frac{1}{4} \frac{\sqrt{\pi}\varepsilon / (\pi^2 (3/2)^{1/4})}{3 + \frac{\pi}{2} \log Q} \quad (57)$$

results in

$$\|f - f'\|_{\ell^\infty} \leq \frac{3\varepsilon}{4} \|\alpha\|_{\ell^1}. \quad (58)$$

We lastly relate f' to $B\alpha$. The definition (56) gives

$$\begin{aligned}
f'_j &= \sum_{q=0}^{Q-1} \sum_{s=0}^S \sum_{t=0}^S \sum_{i=1}^n c_i \alpha_i u_q(\lambda_i) h^{3/2} \frac{(-i)^\ell}{4\pi} w_s Y_\ell^m(\gamma_{s,t}) e^{ix_j \cdot \rho_q \gamma_{s,t}} \\
&= \sum_{i=1}^n c_i h^{3/2} \alpha_i \sum_{q=0}^{Q-1} \sum_{s=0}^S \sum_{t=0}^S u_q(\lambda_i) \frac{(-i)^\ell}{4\pi} w_s Y_\ell^m(\gamma_{s,t}) e^{ix_j \cdot \rho_q \gamma_{s,t}} \\
&= \sum_{i=1}^m c_i h^{3/2} \alpha_i (j_{\ell_i}(r_{x_j} \lambda_i) Y_{\ell_i}^{m_i}(\gamma_{x_j}) + \delta_{i,j}^{\text{dis}}) = (Bf)_j + \sum_{i=1}^m c_i h^{3/2} \alpha_i \delta_{i,j}^{\text{dis}},
\end{aligned} \quad (59)$$

where the third equality follows from Lemma A.1 and $\delta_{i,j}^{\text{dis}}$ is a discretization error that satisfies $\|\delta^{\text{dis}}\|_{\ell^\infty} \leq (3 + \frac{\pi}{2} \log Q) \varepsilon^{\text{dis}}$. This results in

$$\|f' - B\alpha\|_{\ell^\infty} \leq \pi^2 (3/2)^{1/4} \left(3 + \frac{\pi}{2} \log Q\right) \varepsilon^{\text{dis}} \|\alpha\|_{\ell^\infty}. \quad (60)$$

Set

$$\varepsilon^{\text{dis}} = \left(\pi^2 (3/2)^{1/4} \left(3 + \frac{\pi}{2} \log \left[5.3V^{1/3}\right]\right) \right)^{-1} \frac{\varepsilon}{4}. \quad (61)$$

Note that $\varepsilon^{\text{dis}} \leq \varepsilon$ so the assumption $5.3V^{1/3} \geq |\log_2 \varepsilon|$ then implies

$$Q = \log \left[\max\{5.3V^{1/3}, \log_2 \varepsilon^{\text{dis}}\} \right] = \lceil 5.3V^{1/3} \rceil.$$

Combining (60) and (58) gives $\|f - B\alpha\|_{\ell^\infty} = \|\tilde{B}\alpha - B\alpha\|_{\ell^\infty} \leq \varepsilon \|\alpha\|_{\ell^1}$. \square

A.3. Bound on computational complexity of Algorithms 1 and 2.

Claim A.3. *Assume $\lambda \leq 6^{1/3}\pi^{2/3}[(V^{1/3} + 1)/2]$ and $\varepsilon > 0$ is a user-specified accuracy parameter satisfying $|\log_2 \varepsilon| \leq 5.3V^{1/3}$. Then Algorithms 1–2 involve $\mathcal{O}(V(\log V)^2 + V|\log \varepsilon|^2)$ operations.*

Proof of Claim A.3. The NUFFT with n source points and m target points in \mathbb{R}^d and a precision parameter $0 \leq \varepsilon \leq 1$ takes $\mathcal{O}(n \log n + m (\log \frac{1}{\varepsilon})^d)$ operations to achieve ℓ^1 - ℓ^∞ relative error ε (see [4, Eq. (9)] and [5, Sec. 1.1]). For both Algorithms 1 and 2, the number of source points is V and the number of target points is $S(S+1)Q = \mathcal{O}(V)$. In (50) and (57), both algorithms set the precision to $\varepsilon^{\text{nuft}} = \mathcal{O}(\varepsilon/\log Q)$. The computational complexity is therefore $\mathcal{O}(V \log V + V|\log \varepsilon^{\text{nuft}}|^2) = \mathcal{O}(V \log V + V|\log \varepsilon - \log \log Q|^2) = \mathcal{O}(V \log V + V|\log \varepsilon|^2)$ operations.

Algorithms 1 and 2 use the fast spherical harmonics transforms defined in (89) and (90). Each algorithm performs $Q = \mathcal{O}(V^{1/3})$ applications of these transforms, where each application has $\mathcal{O}(S^2)$ grid points and $\mathcal{O}(L^2)$ basis coefficients. With ε^{fsh} from (50) and (57), the computations therefore use $\mathcal{O}(V(\log V)^2 + V|\log \varepsilon^{\text{fsh}}|^2) = \mathcal{O}(V(\log V)^2 + V|\log \varepsilon|^2)$ operations (see [43, 30, 29]).

For fixed ℓ, m , the algorithms perform polynomial interpolation from the $Q = \mathcal{O}(V^{1/3})$ source points to the target points $\lambda_{\ell k}$, where $1 \leq k \leq K$. There are many fast methods for performing interpolation [15, 22, 34, 14, 19, 41]. Using the lowest complexity method of these [14], the cost of each interpolation to ℓ^1 - ℓ^∞ relative precision ε^{in} is $\mathcal{O}(V^{1/3} \log V + K|\log \varepsilon^{\text{in}}|)$. By (24) we have $L, K = \mathcal{O}(V^{1/3})$. There are therefore fewer than $L(2L+1) = \mathcal{O}(V^{2/3})$ interpolation problems, which gives a total complexity of $\mathcal{O}(V \log V + V|\log \varepsilon^{\text{in}}|)$. By (50) and (57), the interpolation step therefore uses $\mathcal{O}(V \log V + V|\log \varepsilon|)$ operations.

All three steps of the algorithm have the computational complexity $\mathcal{O}(V(\log V)^2 + V|\log \varepsilon|^2)$, which concludes the proof of Theorem 3.1. \square

A.4. Auxiliary Lemmas.

Lemma A.1. *Define S and Q as in Lemma 4.2 and 4.1 with accuracy parameter $\eta > 0$. Then for any $i \in \{1, \dots, n\}$, and $j \in \{1, \dots, V\}$*

$$\left| \sum_{q=0}^{Q-1} \sum_{s=0}^S \sum_{t=0}^{S-1} e^{-ix_j \cdot \rho_q \gamma_{s,t}} \frac{i^\ell w_s}{4\pi} \overline{Y_{\ell_i}^{m_i}(\gamma_{s,t})} u_q(\lambda_i) - j_\ell(r_{x_j} \lambda_i) \overline{Y_{\ell}^m(\gamma_{x_j})} \right| \leq \left(3 + \frac{\pi}{2} \log Q\right) \eta,$$

Proof. Putting together Lemma 4.2 and 4.1, we have

$$\begin{aligned} \sum_{q=0}^{Q-1} \sum_{s=0}^S \sum_{t=0}^{S-1} e^{-ix_j \cdot \rho_q \gamma_{s,t}} w_s \overline{Y_{\ell_i}^{m_i}(\gamma_{s,t})} u_q(\lambda_i) &= \sum_{q=0}^{Q-1} \left(j_\ell(r_{x_j} \rho_q) \overline{Y_{\ell_i}^{m_i}(\gamma_{x_j})} + \delta_{qij}^{\text{ang}} \right) u_q(\lambda_i) \\ &= j_\ell(r_{x_j} \lambda_i) \overline{Y_{\ell_i}^{m_i}(\gamma_{x_j})} + \delta_{ij}^{\text{rad}} + \sum_{q=0}^{Q-1} \delta_{qij}^{\text{ang}} u_q(\lambda_i), \end{aligned}$$

where $\delta_{qij}^{\text{ang}}$ and δ_{ij}^{rad} are the approximation errors from Lemma 4.2 and 4.1, respectively. By the choice of Q and S , these approximation errors are controlled by $|\delta_{qij}^{\text{ang}}| \leq \eta$ and $|\delta_{ij}^{\text{rad}}| \leq \eta$. Bounding the term $\sum_{q=0}^{Q-1} |u_q(\lambda_i)|$ as in [47, Eq. (11)],

$$|\delta_{ij}^{\text{rad}} + \sum_{q=0}^{Q-1} \delta_{qij}^{\text{ang}} u_q(\lambda_i)| \leq \eta + \eta(2 + \frac{\pi}{2} \log Q),$$

which finishes the proof. \square

Lemma A.2. *If $\lambda_{\ell k} \leq 6^{1/3}\pi^{2/3}h^{-1}$, then the normalization constants $c_{\ell k}$ in (1) satisfy $c_{\ell k} \leq \pi^2(3/2)^{1/4}h^{-3/2}$.*

Proof of Lemma A.2. By the same argument as in [39, Lemma A.4], we obtain

$$J'_{\ell+1/2}(\lambda_{\ell k})^2 \geq \left(\frac{2}{\pi\lambda_{\ell k}}\right)^2 \frac{2\sqrt{\lambda_{\ell k}^2 - (\ell + 1/2)^2}}{\pi}.$$

Since $\lambda_{\ell k} > \ell + 1/2 + k\pi - \pi/2 + 1/2 > \ell + 2.5$ for $(\ell, k) \in \mathbb{Z}_{\geq 0} \times \mathbb{Z}_{> 0}$ (see [16, Eq. 1.6]), we have $\sqrt{\lambda_{\ell k}^2 - (\ell + 1/2)^2} > \sqrt{6}$. Using this and the assumption $\lambda_{\ell k} \leq 6^{1/3}\pi^{2/3}h^{-1}$ yields

$$c_{\ell k} = \frac{2\sqrt{\lambda_{\ell k}}}{\pi^{1/2}|J'_{\ell+1/2}(\lambda_{\ell k})|} \leq \frac{\pi\lambda_{\ell k}^{3/2}}{2^{1/2}6^{1/4}} \leq \pi^2(3/2)^{1/4}h^{-3/2},$$

as announced. \square

APPENDIX B. SUPPLEMENTARY MATERIALS: CONVENTIONS

This supplement specifies the notational conventions used in the article and includes background material to make the main paper self-contained. Since conventions for special functions and operators used in this paper vary across mathematical communities, care is taken to avoid any potential ambiguity.

B.1. Spherical coordinates. Suppose that $f : \mathbb{R}^3 \rightarrow \mathbb{C}$ and $x = (x_1, x_2, x_3)$ are Cartesian coordinates. Let (r, θ, ϕ) be spherical coordinates defined by

$$\begin{cases} x_1 = r \sin \theta \cos \phi, \\ x_2 = r \sin \theta \sin \phi, \\ x_3 = r \cos \theta, \end{cases} \quad (62)$$

where $r \in [0, \infty)$, $\theta \in [0, \pi]$, and $\phi \in [0, 2\pi)$. More concisely, we can define $\gamma \in \mathbb{S}^2 = \{x \in \mathbb{R}^3 : |x| = 1\}$ by

$$\gamma = (\sin \theta \cos \phi, \sin \theta \sin \phi, \cos \theta), \quad (63)$$

and write $x = r\gamma$. When necessary to avoid ambiguity, we write $r_x, \theta_x, \phi_x, \gamma_x$ to denote the spherical coordinates defined in (62) and (63) corresponding to $x \in \mathbb{R}^3$. The integral of f is expressed in spherical coordinates as

$$\int_{\mathbb{R}^3} f(x) dx = \int_0^{2\pi} \int_0^\pi \int_0^\infty f(r, \theta, \phi) r^2 \sin \theta dr d\theta d\phi = \int_{\mathbb{S}^2} \int_0^\infty f(r\gamma) r^2 dr d\sigma(\gamma),$$

where $d\sigma(\gamma)$ is the surface element on \mathbb{S}^2 . The Laplacian $\Delta = \partial_{x_1 x_1} + \partial_{x_2 x_2} + \partial_{x_3 x_3}$ is expressed in spherical coordinates by

$$\begin{aligned} \Delta &= \partial_{rr} + \frac{2}{r}\partial_r + \frac{1}{r^2} \left(\frac{1}{\sin \theta} \partial_\theta (\sin \theta \partial_\theta) + \frac{1}{(\sin \theta)^2} \partial_{\phi\phi} \right) \\ &= \partial_{rr} + \frac{2}{r}\partial_r + \frac{1}{r^2} \Delta_{\mathbb{S}^2}, \end{aligned} \quad (64)$$

where $\Delta_{\mathbb{S}^2}$ is the Laplace-Beltrami operator on the sphere $\mathbb{S}^2 = \{x \in \mathbb{R}^3 : \|x\| = 1\}$. We define the Fourier-transform of an integrable function $f : \mathbb{R}^3 \rightarrow \mathbb{C}$ using the convention

$$\widehat{f}(\omega) = \int_{\mathbb{R}^3} f(x) e^{-ix \cdot \omega} dx. \quad (65)$$

With this convention, the inverse Fourier transform is given by

$$f(x) = \frac{1}{(2\pi)^3} \int_{\mathbb{R}^3} \widehat{f}(\omega) e^{ix \cdot \omega} d\omega,$$

when f is sufficiently nice, for example when f is in Schwartz space $\mathcal{S}(\mathbb{R}^3)$.

B.2. Spherical Bessel functions. Let j_ℓ denote the ℓ -th order spherical Bessel function of the first kind. We have

$$j_\ell(r) = \left(\frac{\pi}{2r}\right)^{1/2} J_{\ell+1/2}(r), \quad (66)$$

where J_q is the q -th order Bessel function of the first kind, see [11, Eq. 10.47.3]. Further, j_ℓ satisfies the differential equation

$$-\left(\partial_{rr} + \frac{2}{r} + \frac{\ell(\ell+1)}{r^2}\right)j_\ell(r) = j_\ell(r), \quad (67)$$

see [11, 10.47.1].

B.3. Spherical harmonics. Let $Y_\ell^m(\theta, \phi)$ be (normalized) spherical harmonics defined by

$$Y_\ell^m(\theta, \phi) = \left(\frac{(\ell-m)!(2\ell+1)}{4\pi(\ell+m)!}\right)^{1/2} e^{im\phi} P_\ell^m(\cos\theta), \quad (68)$$

for $m \in \{-\ell, \dots, \ell\}$ and $\ell \in \mathbb{Z}_{\geq 0}$, see [11, Eq. 14.30.1]. Here, P_ℓ^m denotes the associated Legendre function of the first kind, see [11, Eq. 14.3.6]. With the above normalization, the spherical harmonics satisfy the identity

$$\int_0^{2\pi} \int_0^\pi Y_{\ell_1}^{m_1}(\theta, \phi) \overline{Y_{\ell_2}^{m_2}(\theta, \phi)} \sin\theta d\theta d\phi = \delta_{\ell_1, \ell_2} \delta_{m_1, m_2}, \quad (69)$$

where $\delta_{\ell_1, \ell_2} = 1$ if $\ell_1 = \ell_2$ and 0 if $\ell_1 \neq \ell_2$, see [11, Eq. 14.30.8]. Additionally, the Y_ℓ^m satisfy

$$\sum_{m=-\ell}^{\ell} |Y_\ell^m(\theta, \phi)|^2 = \frac{2\ell+1}{4\pi},$$

which is known as Unsöld's identity [10, Eq. (4.37)] and follows from the addition theorem

$$P_\ell(\gamma_1 \cdot \gamma_2) = \frac{4\pi}{2\ell+1} \sum_{m=-\ell}^{\ell} Y_\ell^m(\gamma_1) \overline{Y_\ell^m(\gamma_2)},$$

for $\gamma_1, \gamma_2 \in \mathbb{S}^2$. See also [52, Corollary IV.2.9b]. In particular, it follows that for all θ and ϕ

$$|Y_\ell^m(\theta, \phi)| \leq \sqrt{\frac{2\ell+1}{4\pi}}, \quad \text{for any } \ell, m \text{ with } -\ell \leq m \leq \ell. \quad (70)$$

Further, spherical harmonics satisfy the differential equation

$$-\left(\frac{1}{\sin\theta} \partial_\theta (\sin\theta \partial_\theta) + \frac{1}{(\sin\theta)^2} \partial_{\phi\phi}\right) Y_\ell^m(\theta, \phi) = \ell(\ell+1) Y_\ell^m(\theta, \phi), \quad (71)$$

see [11, Eq. 14.30.10], which can be written concisely as

$$-\Delta_{\mathbb{S}^2} Y_\ell^m = \ell(\ell+1) Y_\ell^m. \quad (72)$$

In other words, the functions Y_ℓ^m are eigenfunctions of the operator $-\Delta_{\mathbb{S}^2}$ with eigenvalue $\ell(\ell+1)$ for $\ell, m \in \mathbb{Z}$ such that $|m| \leq \ell$.

Remark B.1 (Real-valued spherical harmonics). Real-valued spherical harmonics $\tilde{Y}_\ell^m : \mathbb{S}^2 \rightarrow \mathbb{R}$ can be obtained by taking linear combinations of Y_ℓ^m as follows:

$$\tilde{Y}_\ell^m = \begin{cases} \frac{i}{\sqrt{2}} \left(Y_\ell^{-|m|} - (-1)^m Y_\ell^{|m|} \right) & \text{if } m < 0 \\ Y_\ell^0 & \text{if } m = 0 \\ \frac{1}{\sqrt{2}} \left(Y_\ell^{-|m|} + (-1)^m Y_\ell^{|m|} \right) & \text{if } m > 0. \end{cases} \quad (73)$$

Indeed, the fact that \tilde{Y}_ℓ^m is real-valued follows from the definition (68) of Y_ℓ^m and the identity

$$P_\ell^{-m}(x) = (-1)^m \frac{(\ell - m)!}{(\ell + m)!} P_\ell^m(x);$$

see [11, Eq. (14.9.3)]. The functions \tilde{Y}_ℓ^m are orthonormal on \mathbb{S}^2 .

B.4. Ball harmonics. The harmonics on the unit ball $\mathbb{B} = \{x \in \mathbb{R}^3 : \|x\| < 1\}$ in \mathbb{R}^3 are eigenfunctions of the Dirichlet Laplacian, i.e., they solve the eigenproblem

$$\begin{cases} -\Delta\psi = \lambda\psi & \text{in } \mathbb{B}, \\ \psi = 0 & \text{on } \partial\mathbb{B}, \end{cases} \quad (74)$$

where $\partial\mathbb{B} = \mathbb{S}^2$ denotes the boundary of \mathbb{B} . The eigenfunctions of the Laplacian form an orthonormal basis of square-integrable functions on \mathbb{B} and can be expressed by

$$\psi_{k,\ell,m}(r, \theta, \phi) = c_{\ell k} j_\ell(\lambda_{\ell k} r) Y_\ell^m(\theta, \phi) \chi_{[0,1)}(r), \quad (75)$$

for $m \in \{-\ell, \dots, \ell\}$, $\ell \in \mathbb{Z}_{\geq 0}$, and $k \in \mathbb{Z}_{> 0}$, where $c_{\ell k}$ are positive normalization constants ensuring $\|\psi_{k,\ell,m}\|_{L^2} = 1$, and the constant $\lambda_{\ell k}$ is the k -th positive root of j_ℓ ; see for example [21, §3.3]. The inclusion of the indicator function $\chi_{[0,1)}(x)$ for $[0, 1)$ extends the domain of the ball harmonics to \mathbb{R}^3 by setting the value equal to zero outside of \mathbb{B} .

Note that by (66) the constant $\lambda_{\ell k}$ can equivalently be defined as the k -th positive root of $J_{\ell+1/2}$ by (66). Moreover, it holds

$$-\Delta\psi_{k,\ell,m} = \lambda_{\ell k}^2 \psi_{k,\ell,m},$$

so that $\lambda_{\ell k}^2$ is the eigenvalue associated with the eigenfunctions $\psi_{k,\ell,m}$ of the operator $-\Delta$. Indeed, this is straightforward to see by writing the Laplacian in spherical coordinates:

$$\Delta = \partial_{rr} + \frac{2}{r}\partial_r + \frac{1}{r^2}\Delta_{\mathbb{S}^2},$$

where $\Delta_{\mathbb{S}^2}$ is the Laplace Beltrami operator on the sphere. This gives

$$\begin{aligned} \Delta\psi_{k,\ell,m} &= \lambda_{\ell k}^2 j_\ell''(\lambda_{\ell k} r) Y_\ell^m + \frac{2\lambda_{\ell k}}{r} j_\ell'(\lambda_{\ell k} r) Y_\ell^m + j_\ell(\lambda_{\ell k} r) \frac{1}{r^2} \Delta_{\mathbb{S}^2} Y_\ell^m \\ &= \left(\lambda_{\ell k}^2 j_\ell''(\lambda_{\ell k} r) + \frac{2\lambda_{\ell k}}{r} j_\ell'(\lambda_{\ell k} r) - \frac{\ell(\ell+1)}{r^2} j_\ell(\lambda_{\ell k} r) \right) Y_\ell^m(\theta, \phi) \\ &= -\lambda_{\ell k}^2 j_\ell(\lambda_{\ell k} r) Y_\ell^m = -\lambda_{\ell k}^2 \psi_{k,\ell,m}, \end{aligned} \quad (76)$$

where the final equality follows from (67), and $f' := \partial_r f$ and $f'' := \partial_{rr} f$. Finally, we define the normalization constants $c_{\ell k}$ for completeness. We have

$$\begin{aligned} \|\psi_{k,\ell,m}\|_{L^2}^2 &= c_{\ell k}^2 \int_0^{2\pi} \int_0^\pi \int_0^1 j_\ell(\lambda_{\ell k} r)^2 |Y_\ell^m(\theta, \phi)|^2 r^2 \sin\theta dr d\theta d\phi \\ &= c_{\ell k}^2 \int_0^1 j_\ell(\lambda_{\ell k} r)^2 r^2 dr = c_{\ell k}^2 \int_0^1 \frac{\pi}{2\lambda_{\ell k}} J_{\ell+1/2}(\lambda_{\ell k} r)^2 r dr \\ &= \frac{\pi c_{\ell k}^2}{4\lambda_{\ell k}} (J'_{\ell+1/2}(\lambda_{\ell k}))^2, \end{aligned} \quad (77)$$

where the final equality follows from [11, Eq. 10.22.37]. Thus,

$$c_{\ell k} = \frac{2\sqrt{\lambda_{\ell k}}}{\pi^{1/2} |J'_{\ell+1/2}(\lambda_{\ell k})|}. \quad (78)$$

Remark B.2 (Real-valued ball harmonics). Note that while the ball harmonics $\psi_{k,\ell,m}$ are complex-valued, orthonormal real-valued analogs $\tilde{\psi}_{k,\ell,m}$ can be obtained by defining

$$\tilde{\psi}_{k,\ell,m} = \begin{cases} \frac{i}{\sqrt{2}} (\psi_{k,\ell,-|m|} - (-1)^m \psi_{k,\ell,|m|}) & \text{if } m < 0 \\ \psi_{k,\ell,0} & \text{if } m = 0 \\ \frac{1}{\sqrt{2}} (\psi_{k,\ell,-|m|} + (-1)^m \psi_{k,\ell,|m|}) & \text{if } m > 0; \end{cases} \quad (79)$$

the fact that $\tilde{\psi}_{k,\ell,m}$ is real-valued follows from (73).

B.5. Quadrature on \mathbb{S}^2 . We define a quadrature rule on the sphere that is exact for integrals corresponding to inner products of functions that have bandlimited spherical harmonic expansions. We define quadrature nodes $\gamma_{s,t} \in \mathbb{S}^2$ by

$$\gamma_{s,t} = (\sin \theta_s \cos \phi_t, \sin \theta_s \sin \phi_t, \cos \theta_s), \quad (80)$$

where

$$(\theta_s, \phi_t) := \left(\frac{\pi s}{S}, \frac{2\pi t}{S} \right) \quad \text{for } (s, t) \in \{0, \dots, S\} \times \{0, \dots, S-1\}. \quad (81)$$

We define quadrature weights w_s equal to the Clenshaw-Curtis quadrature with respect to θ_s and uniform quadrature with respect to ϕ_t . The quadrature weights w_s are given by

$$w_s := \frac{4\pi \varepsilon_s}{S^2} \sum_{u=0}^{\lfloor S/2 \rfloor} \frac{2\varepsilon_u}{1-4u^2} \cos\left(\frac{2\pi s u}{S}\right), \quad \text{for } s \in \{0, \dots, S\}, \quad (82)$$

where $\varepsilon_0 = \varepsilon_S = 1/2$ and $\varepsilon_u = 1$ otherwise, see [41, 53]. We say that $f : \mathbb{S}^2 \rightarrow \mathbb{C}$ is bandlimited on the sphere if

$$f(\gamma) = \sum_{\ell=0}^L \sum_{m=-\ell}^{\ell} \alpha_{\ell,m} Y_{\ell}^m(\gamma), \quad (83)$$

for some coefficients $\alpha_{\ell,m}$. Suppose that $f, g : \mathbb{S}^2 \rightarrow \mathbb{C}$ are bandlimited on the sphere in the sense of (83) for $L \leq S/2$. Then,

$$\sum_{s=0}^S \sum_{t=0}^{S-1} f(\gamma_{s,t}) \overline{g(\gamma_{s,t})} w_s = \int_{\mathbb{S}^2} f(\gamma) \overline{g(\gamma)} d\sigma(\gamma), \quad (84)$$

see [41, Theorem 9.60] (see also [13, 44]). We note that the quadrature weights w_s satisfy the bound

$$|w_s| \leq \frac{4\pi}{S^2} \left(1 + \sum_{u=1}^{\infty} \frac{2}{4u^2 - 1} \right) = \frac{8\pi}{S^2}, \quad \text{for } s \in \{0, \dots, S\}, \quad (85)$$

where the equality follows from the fact that the sum telescopes. We also note that $w_s \geq 0$ holds, since

$$w_s \geq \frac{4\pi}{S^2} \left(1 - \sum_{u=1}^{\infty} \frac{2}{4u^2 - 1} \right) = 0. \quad (86)$$

Remark B.3 (Choice of quadrature). In related works, different authors use different quadrature points $\gamma_{s,t}$ and weights $w_{s,t}$ on the sphere. For example, another choice is Gaussian quadrature nodes in the variable t , see [48]. This paper assumes the product Clenshaw-Curtis quadrature defined in §B.5 above for the sake of definiteness. However, straightforward modifications to the theory and implemented code could be performed to extend our results to other quadrature choices.

B.6. Spherical harmonic transforms. We use two types of spherical harmonics transforms between coefficients $(\beta_{\ell,m})$ and function values $(a_{s,t})$, where (ℓ, m) range over

$$(\ell, m) \in \{(\ell, m) \in \mathbb{Z}^2 : 0 \leq \ell \leq L, \text{ and } -\ell \leq m \leq \ell\}, \quad (87)$$

and (s, t) range over

$$(s, t) \in \{0, \dots, S\} \times \{0, \dots, S-1\}. \quad (88)$$

The first kind of spherical harmonics transform maps coefficients $(\beta_{\ell,m})$ to function values $(a_{s,t})$ via

$$(\beta_{\ell,m}) \mapsto a_{s,t} := \sum_{\ell=0}^L \sum_{m=-\ell}^{\ell} \beta_{\ell,m} Y_{\ell}^m(\gamma_{s,t}), \quad (89)$$

where $\gamma_{s,t}$ are defined in (81). The second kind of spherical harmonics transform maps function values $(a_{s,t})$ to coefficients by $(\tilde{\beta}_{\ell,m})$ via

$$(a_{s,t}) \mapsto \tilde{\beta}_{\ell,m} := \sum_{s=0}^S \sum_{t=0}^{S-1} a_{s,t} \overline{Y_{\ell}^m(\gamma_{s,t})} w_s, \quad (90)$$

where w_s are the quadrature weights defined in (82).

B.7. Fast spherical harmonic transforms. If the number of coefficients described by the index sets (87) and (88) are both order N , then directly computing the transforms $(\beta_{\ell,m}) \mapsto (a_{s,t})$ and $(a_{s,t}) \mapsto (\tilde{\beta}_{\ell,m})$ defined by (89) and (90) would require order N^2 operations. Fast spherical harmonic transforms like [48, 51] compute these transforms in $\mathcal{O}(N \log N)$ operations. We note that in practice, however, there are $\mathcal{O}(N^{3/2} \log N)$ implementations [8] that have better running time constants and thus are more practical for small to moderate input sizes. The code accompanying our paper allows the user to choose between asymptotically fast [51] and asymptotically slow (but in practice fast) [8] spherical harmonics transforms at runtime.

Email address: `jkileel@math.utexas.edu`

Email address: `marsnich@oregonstate.edu`

Email address: `hm6655@princeton.edu`

Email address: `amits@math.princeton.edu`